SOUTHEASTERN GEOLOGY

PUBLISHED AT DUKE UNIVERSITY DURHAM, NORTH CAROLINA

VOL. 15 NO. 2 JULY, 1973

SOUTHEASTERN GEOLOGY

PUBLISHED QUARTERLY

AT

DUKE UNIVERSITY

This journal welcomes original papers on all phases of geology, geophysics, and geochemistry as related to the Southeast. Transmit manuscripts to S. DUNCAN HERON, JR., BOX 6665, COLLEGE STATION, DURHAM, NORTH CAROLINA. Please observe the following:

(1) Type the manuscript with double space lines and submit in duplicate.
(2) Cite references and prepare bibliographic lists in accordance with the method found within the pages of this journal.
(3) Submit line drawings and complex tables as finished copy.
(4) Make certain that all photographs are sharp, clear, and of good contrast.
(5) Stratigraphic terminology should abide by the Code of Stratigraphic Nomenclature (AAPG, v. 45, 1961).

Proofs will not be sent authors unless a request to this effect accompanies the manuscript.

Reprints must be ordered prior to publication. Prices are available upon request.

* * * * * *

Subscriptions to Southeastern Geology are $5.00 per volume. Inquiries should be addressed to WM. J. FURBISH, BUSINESS AND CIRCULATION MANAGER, BOX 6665, COLLEGE STATION, DURHAM NORTH CAROLINA. Make check payable to Southeastern Geology.

SOUTHEASTERN GEOLOGY

Table of Contents

Vol. 15, No. 2

1973

ANALYSIS OF CHEMICAL AND PALEOTEMPERATURE DATA FROM SELECTED CARBONATE ROCKS OF THE SOUTHERN APPALACHIANS

By

Robert D. Hatcher, Jr.
Vaneaton Price, Jr.
David S. Snipes

Department of Chemistry and Geology
Clemson University
Clemson, South Carolina 29631

ABSTRACT

Several trace, minor, and major elements (Mn, Sr, Zn, Cu, Pb, Li, Fe, Ca and Mg) have been determined in the acid soluble portion of 67 carbonate rock samples from the southern Appalachians. X-ray diffraction (magnesian calcite) determinations of paleotemperatures have also been made.

Generally, each lithologic unit (e.g., Murphy marble, Ocoee carbonates, Kings Mountain belt marbles, Chauga River Formation marbles) exhibits a characteristic range of paleotemperatures and elemental concentrations. Brevard (Chauga River Formation) carbonates contain larger quantities of Mn, Sr, Zn and Fe than does any other group. The present data support earlier field and petrologic studies indicating that tectonic slice carbonates of the South Carolina Brevard Zone are different from Chauga River and nearby Poor Mountain carbonates. Kings Mountain belt marbles are relatively impoverished in Mn and Sr but are enriched in Fe. Shady and Murphy samples are low in Sr and contain moderate amounts of Mn and Fe.

Paleotemperatures above 500°C are recorded by many Chauga River samples and are attributed to short-term frictional heating during faulting which post-dated regional metamorphism and was not accompanied by re-equilibration of adjacent pelitic metamorphic assemblages. Many carbonate temperatures in this study are lower than that inferred from mineral assemblages in nearby pelitic rocks. These may be either cooling temperatures and not representative of the regional metamorphic thermal peak or may represent a later lower temperature thermal event.

INTRODUCTION

This study began as an attempt to confirm or deny certain conclusions drawn by Hatcher (1971) in a field and petrologic study of the

Brevard Zone. The investigation grew from an attempt to characterize carbonate rocks occurring within or close to the Brevard Zone according to their trace and minor element content into a study of selected trace, minor and major element concentrations and paleotemperatures in carbonate rock samples from across the crystalline southern Appalachians, and the Valley and Ridge. Several control samples were added from central Tennessee. The purpose of the investigation evolved from one of determining distinctive characteristics over a small area to attempting to correlate rock units over a wide area using trace and minor elements. We know of no previous attempts to correlate carbonate rocks of the southern Appalachians using our techniques.

Sixty-seven samples were studied in this investigation. They were obtained from all major carbonate rock units in the southern crystalline Appalachians except the Talladega. Figure 1 shows the locations of sampling sites. Trace, minor and major elements were determined by atomic absorption while paleotemperatures were determined by X-ray diffraction. Data were then processed by cluster analysis to aid in interpretation.

Acknowledgments

Many of the samples were collected during the course of geologic mapping by Hatcher with support of the National Science Foundation (Grants GA-1409 and GA-20321), South Carolina Division of Geology and the Georgia Geological Survey. Other contributors of samples include R. E. Lemmon, J. R. Butler, L. S. Wiener, T. L. Neathery, F. H. Manley, W. R. Power and the Tennessee Valley Authority. F. H. Manley (oral comm., 1971; Manley and Power, 1972) introduced us to the paleotemperature technique which Snipes (in preparation) has refined and modified. Furman University and Clemson University contributed computer time. Louis Schafter, Furman University geology undergraduate wrote the cluster analysis program. David Dalsis of the Clemson University Chemistry Department performed the wet analyses. Critical review by P. C. Ragland is gratefully acknowledged.

TECHNIQUES

Elemental Analyses

All analyses used for correlation in this study were made by atomic absorption spectrophotometry. Standards included Dolomite 400 and Limestone 401 prepared by the G. F. Smith Chemical Company, NBS 1a, a limestone sample distributed by the National Bureau of Standards, and salt curves prepared in a stock solution of Johnson and Mathey spectrographically pure calcium carbonate and magnesium metal.

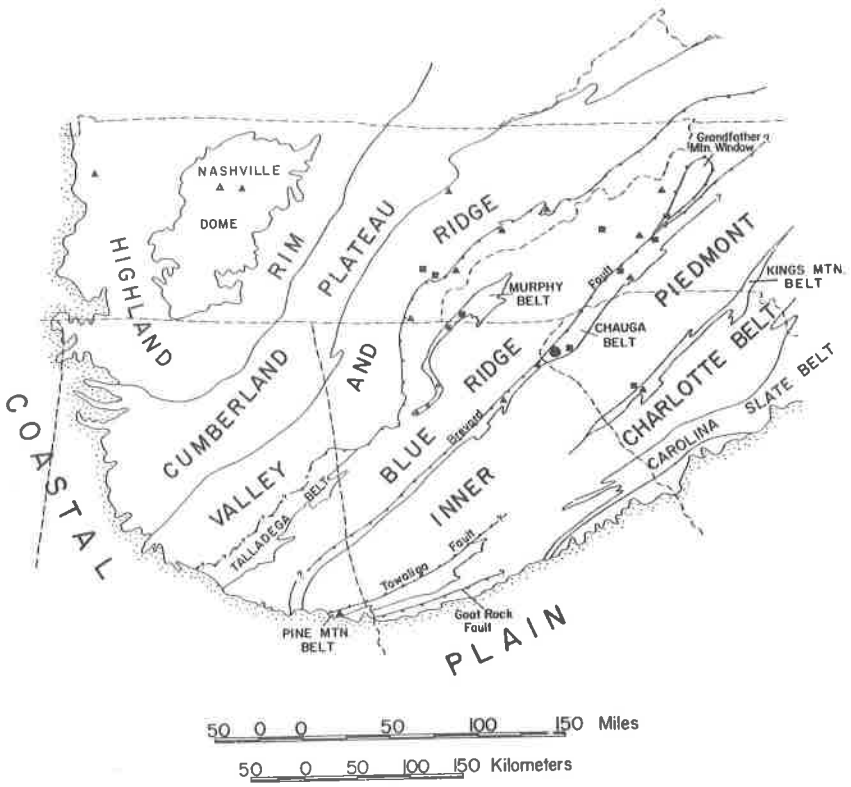

Figure 1. Map showing the different geologic provinces in the southeast and the sample localities. The triangles indicate one sample was collected at a locality, the squares indicate 2-6 samples and the large circle indicates ≥ 6 samples.

With slight variations the samples were all ground to pass a 100-mesh seive, 1.0 gram was dissolved in 20 percent HCl and 2-3 drops of HNO_3 by heating for ten minutes. This solution was diluted to 100 ml for determination of minor and trace elements. Further dilution was necessary in order to analyze for Ca and Mg.

An insoluble residue remained in many samples. Comparison of elemental data (Fe, Mg, trace elements) with percentages of oqaques, chlorite and biotite in 16 published modal analyses of our samples (Hatcher, 1971, Appendices 1a, 1b and 1c) indicates that the insoluble residues with one exception do not contribute to the solute. There is a correlation between percentage of opaques and the amount of iron in solution (correlation coefficient = 0.73). We feel that it is consistent with the purposes of the present study to consider any contribution simply as an attribute of the sample.

When calculated as RCO_3, the analysis weights generally corroborate the predominantly carbonate nature of the samples. The lowest

Table 1. Comparison of Wet Chemical and Atomic Absorption Analyses.

Obs. #	CaO		MgO		Fe_2O_3	
	1[a]	2[b]	1	2	1	2
1	11.84	14.7	2.14	2.31	5.76	2.93
43	36.53	35.1	< 0.2	0.22	0.89	0.6
49	26.72	24.8	1.41	1.43	4.23	2.93
52	17.76	17.0	1.78	1.54	2.63	1.93
53	48.17	48.0	0.31	0.56	0.54	0.47
57	30.88	28.3	1.96	1.86	2.60	1.57

[a]Wet chemical analyses (total rock).
[b]Atomic absorption analyses.

RCO_3 sum is 20 percent; 94 percent of the samples sum to > 50 percent total carbonates and 73 percent of the samples sum to > 90 percent total carbonates. Nineteen samples (28%) sum to > 95 percent. Analytical precision for all elements is generally better than 5 percent.

Duplication wet-chemical analyses were available for six samples and the results compare favorably except for Fe_2O_3 (Table 1). The lower values for Fe_2O_3 found by atomic absorption analysis are due to the fact that a large proportion of the iron is in minerals of the insoluble residue, e. g., biotite, which are taken into solution in the wet analysis.

Paleotemperatures

Graf and Goldsmith (1958) have published data on the magnesian calcite-dolomite solvus which permits the mole percent Mg in calcite in the presence of dolomite to be interpreted as a function of paleotemperature. We have used the X-ray diffraction method of Graf and Goldsmith (1958) in which silicon is used as an internal standard to determine the mole percent $MgCO_3$ in calcite. The mole percent values are converted into temperature values using the data of Graf and Goldsmith (1958) and Goldsmith and Newton (1969). Curves for both steps were prepared by least squares methods (Snipes, in preparation).

Some problems in the application of the calcite-dolomite solvus to natural samples are:

1. Mg deficiency. Unless there is sufficient initial dolomite present any derived metamorphic temperature will be too low.
2. Substitution of Fe^{+2} or Mn^{+2} in the calcite instead of Mg^{+2} will yield temperatures which are too low (Goldsmith and others, 1955).
3. Weathering tends to selectively remove Mg and gives low

results; therefore only fresh samples should be used (Goldsmith and others, 1955).

Cluster Analysis

Cluster analysis is a technique used to look for groups in ungrouped data. There are several methods in the literature (see Parks, 1966). We have chosen to use the method of distance functions where the distance, D, between any two points $P_i(q_i, r_i, \ldots, z_i)$ and P_j $(q_j, r_j, \ldots, z_j)$ is defined as

$$D = \sqrt{(q_i-q_j)^2 + (r_i-r_j)^2 + \ldots + (z_i-z_j)^2}.$$

The coordinates (q, r, ..., z) are measured attributes of k samples. The attributes are quantifiable variables such as chemical element concentrations, as in this paper. The points (P_1, P_2, ..., P_k) are the positions of the samples in n-dimensional space. Thus a distance, D, can be calculated between any two points having n measured variables.

The technique of clustering we used calculates D values and saves those below a certain specified value. Sample pairs with small D values are then averaged and considered as single samples for a recalculation of D values. The process is continued with storage of pairs and increase of the level for saving D's until all samples are grouped. The grouped samples are then graphed as a dendrogram (Figure 2) with lines connecting sample pairs at the appropriate D level.

The clustering technique assembles n-dimensional data into an easily read 2-dimensional graph. It does not make statistical judgments about the significance of any groupings.

DISCUSSION OF RESULTS

Our samples were collected from several geologic terranes or units. These are (Figure 1, west to east):

1. Craton
2. Copper Ridge Dolomite
3. Shady Dolomite
4. Murphy belt
5. Blue Ridge samples from several areas in western N. C. of unknown affiliations. They may in part be Ocoee equivalents.
6. Ocoee Supergroup.
7. Chauga River. This is the stratigraphic carbonate of the Brevard Zone (Hatcher, 1969).
8. Slice. Typically dolomitic tectonic slices associated with the Brevard cataclastic zone (see Hatcher, 1971, Figure 2).
9. Poor Mountain Formation (Hatcher, 1969).
10. Kings Mountain belt. No samples were collected from the Gaffney Marble at Kings Mountain, North Carolina.

Table 2. Analytical Data and Sample Localities (Elemental Data in ppm Unless Otherwise Noted).

Observation #	Lithology Belt and/or Age	Locality or Station # or other	Pb	Mn	Cu	Sr	Zn	Li	Fe	% Ca	% Mg	Ca/Mg	T°C	Metamorphic Grade[a]	Dolomite Present[a]	Remarks
1	Blue Ridge Ocoee (Brevard type)	Black Mtn., North Carolina	--	920	46	100	43.5	15.6	20,500	10.57	1.39	7.604	543	medium	no	
2	Blue Ridge Ocoee	U.S.#4 Parksville, Tenn	--	65	6	360	24.7	1.7	3,500	38.23	0.57	67.07	225	Low to Unmeta	no	
3	Blue Ridge Bandane	Near Spruce Pine, N.C.	--	37	0	50	7.8	1.2	135	20.67	13.17	1.569	not obs.	Med-high	yes	
4	Blue Ridge Leicester #1	Madison Co., N.C.	20	820	--	75	2	--	4,800	36.15	0.3	120.0	<140	Med-high	no	
5	Blue Ridge Leicester #2	Madison Co., N.C.	--	800	--	35	<1	--	5,150	26.29	0.3	88.0	<140	Med-high	no	
6	Blue Ridge Lansing	Ashe Co., N.C.	--	2,750	--	18	2	--	24,700	23.0	8.93	2.6	624.4	Med-high	no	Ankerite
7	Blue Ridge Leicester #3	Madison Co., N.C.	20	2,180	--	135	<1	--	15,250	42.72	0.4	107.0	245	Med-high	no	Rhomb
8	Ocoee Walden Creek Group	Citico Ck., Monroe Co., Tenn.	--	490	--	1,400	6	--	4,800	37.08	0.8	46.0	<140	low	yes	
9	Kings Mtn. Belt	Masters Kiln, Laurens Co.,S.C.	--	99	1.9	160	9.2	2.7	4,700	37.45	1.15	32.565	145	low-med	no	
10	Kings Mtn. Belt, S.C.	SM26A[b]	--	15	0.9	590	20.5	1.2	280	39.16	0.30	130.533	<140	low-med.	no	
11	Kings Mtn. Belt, S.C.	SM26B[b]	--	132	1.9	540	9.5	1.2	2,000	36.21	0.37	97.865	<140	low-med	no	
12	Kings Mtn. Belt, S.C.	S26-315[b]	11	410	0	490	0	--	2,460	34.50	0.68	50.735	<140	med-high	no	
13	Kings Mtn. Belt, S.C.	S25-371A[b]	11.7	370	0	340	0	--	2,000	33.26	0.37	89.892	<140	med-high	no	
14	Kings Mtn. Belt, S.C.	S25-810A[b]	14	450	0	150	0	--	1,080	34.81	0.54	64.463	<140	med-high	no	
15	Kings Mtn. (Pine Mtn)Belt	Chewacla Alabama	--	40	0	50	6.8	1.3	120	24.09	13.17	1.829	Not Obs.	low-med	yes	
16	Newman Ls. (Miss.)	Rockwood, Tenn.	--	62	3.8	300	10.6	7.6	1,280	37.45	0.73	51.301	<140	Unmeta.	no	
17	Hermitage Lam. Argill(Ord)	Nashville, Tenn.	--	143	1.2	160	10.8	2.5	7,400	13.52	1.39	9.727	271	Unmeta.	yes	
18	Carters Ls. (Ord.)	Lebanon, Tenn.	9	95	0	220	2	--	2,000	33.26	2.29	14.524	198	Unmeta.	yes	

Table 2 con't.

19	Warsaw Ls. (Miss.)	Waverly, Tenn.	9.4	40	0	180	4	--	1,300	27.82	4.05	6.869	200	Unmeta.	yes
20	Murphy (Tate) Marble	Waleska-Pine Log, Ga.	—	74	1.9	1,520	9.7	1.2	2,550	36.05	0.44	81.932	<140	low-med.	no
21	Murphy (Tate)Marble	County Quarry, Mineral Bluff,Ga	--	236	1.9	70	8.5	4.4	1,550	21.45	11.57	1.854	259	low-med.	yes
22	Murphy (Pink) (Tate) Marble	Tate, Ga.	—	77	1.9	220	10.9	1.2	1,800	34.35	1.24	27.702	403	low-med.	no
23	Murphy (Tate) Marble	Campbell Quarry, Mineral Bluff,Ga.	—	174	1.9	70	9.0	2.9	1,550	24.24	11.20	2.164	328	low-med.	yes
24	Murphy (Tate) Marble	Marble Hill, Ga.	—	85	3.9	100	10.9	1.7	860	41.65	2.61	15.958	347	low-med	yes
25	Murphy Marble(light)	Murphy-Andrews, N.C.	11	320	0	50	0	--	1,500	22.69	13.17	1.723	337	low-med	yes
26	Murphy Marble(dark)	Murphy-Andrews, N.C.	9	6,100	2	40	0	--	16,000	20.36	11.47	1.775	470	low-med	yes
27	Shady dol. Cs-1	Tellico Plains, Tenn	--	240	6	0	7.8	1.4	1,500	20.83	12.05	1.729	Not Obs.	Unmeta.	yes
28	Shady dol. Cs-2	Tellico Plains, Tenn.	--	371	1.9	50	7.3	1.2	2,000	18.96	12.37	1.533	Not Obs.	Unmeta.	yes
29	Shady dol. Cs-3	Tellico Plains, Tenn.	--	280	23.4	0	11.4	1.2	1,720	19.73	12.27	1.608	Not Obs.	Unmeta.	yes
30	Shady dol. Cs-4	Tellico Plains, Tenn.	--	378	28.3	0	7.5	1.2	3,500	18.34	11.57	1.585	Not Obs.	Unmeta.	yes
31	Shady dol. I-40	Newport, Tenn .	10	168	3	0	8.3	0.7	1,830	19.27	12.09	1.594	Not Obs.	Unmeta.	yes
32	Shady dol. Tenna. 73	Townshend, Tenn.	—	138	1.9	50	8.7	1.8	570	21.45	13.34	1.608	Not Obs.	Unmeta.	yes
33	Shady dol. GMW (light)	Linville, N.C.	12	440	0	85	0	--	4,400	18.96	12.37	1.533	Not Obs.	Unmeta. to low	yes
34	Shady dol. GMW (dark)	Linville, N.C.	11	300	0	70	3	-20	2,950	19.58	11.41	1.716	Not Obs.	Unmeta. to low	yes
35	Copper Ridge Dol. Ccr-1	Englewood, Tenn.	--	37	30.5	145	7.8	10.0	250	24.56	12.21	1.766	212	Unmeta.	yes
36	Copper Ridge Dol. Ccr-2	Englewood, Tenn.	--	37	4	100	7.8	26.8	480	27.19	8.80	3.090	<140	Unmeta.	yes
37	Shady Slice 699-1a	Brevard Zone, S.C.	--	238	1.9	250	35.8	3.4	5,800	36.68	8.16	4.495	173	Unmeta. to low	yes
38	Shady Slice 699-1b	Brevard Zone, S.C.	5.5	151	147	635	10.8	21.5	430	19.27	5.44	3.542	194	Unmeta. to low	yes

Table 2 con't.

			Pb	Mn	Cu	Sr	Zn	Li	Fe	% Ca	% Mg	Ca/Mg	T°C	Metamorphic Grade[a]	Dolomite Present?
39	Shady Slice 699-2[c]	Brevard Zone, S.C.	--	131	1.9	320	14.0	13.7	1,600	18.96	6.93	2.736	307	Unmeta. to low	yes
40	Shady Slice 699-3[c]	Brevard Zone, S.C.	--	598	1.9	360	13.8	1.2	2,100	22.22	2.67	8.322	<140	Unmeta. to low	yes
41	Shady (?) 411[c]	Brevard Zone, S.C.	--	82	255	180	16.5	2.7	2,800	22.38	11.09	2.018	317	Unmeta. to low	yes
42	Shady Slice[d]	Hot Springs Bath House, N.C.	11	340	0	35	1	--	2,000	21.76	12.91	1.686	Not Obs.	Unmeta. to low	yes
43	Poor Mountain Marble 40[c]	Poor Mtn., S.C.	--	298	17.2	80	9.0	1.2	4,200	24.40	0.13	187.69	<140	low to med.	no
44	Poor Mtn. Marble 766A[c]	Hurricane Mtn., S.C.	--	110	10	310	13.8	3.7	10,400	37.30	0.80	71.731	450	low to med.	no
45	Poor Mtn. Marble 300[c]	Cedar Creek, S.C.	--	104	13.2	300	10.9	2.7	10,400	29.37	0.49	59.939	324	low to med.	no
46	Poor Mtn. Marble(?) N9-24[d]	Chimney Rock, N.C.	14	450	3	210	5	-20	6,600	34.50	0.26	132.692	237	low to med.	no
47	Chauga River 634[c]	Brevard Zone, S.C.	--	208	6	205	31.8	21.7	14,000	10.26	0.71	14.451	572	low to med.	no
48	Chauga River 646[c]	Brevard Zone, S.C.	--	438	35.0	0	33.0	27.8	16,600	9.36	1.41	6.638	633	low to med.	no
49	Chauga River 666[c]	Brevard Zone, S.C.	10	470	4.5	700	33.8	18.3	20,500	17.72	0.87	20.368	442	low to med.	no
50	Chauga River 686[c]	Brevard Zone, S.C.	--	477	8.3	50	33.5	30.8	14,000	11.50	1.47	7.823	606	low to med.	no
51	Chauga River 688[c]	Brevard Zone, S.C.	--	216	4.8	145	28.0	14.9	15,300	9.79	0.89	11.00	539	low to med.	no
52	Chauga River 406 gray[c]	Brevard Zone, S.C.	--	519	67.8	50	24.5	7.4	13,400	12.12	0.93	13.032	567	low to med.	no
53	Chauga River 406 White[c]	Brevard Zone, S.C.	--	398	36.9	90	13.5	0.5	3,300	34.35	0.34	101.029	218	low to med.	no
54	Chauga River 4[c]	Brevard Zone, S.C.	--	313	7	360	35.5	15.9	18,500	12.59	0.96	13.115	553	low to med.	no
55	Chauga River 508[c]	Brevard Zone, S.C.	--	232	10.0	100	39.3	39.8	24,000	8.24	1.07	7.701	512	low to med.	no
56	Chauga River TL-63[c]	Brevard Zone, S.C.	--	209	4.9	1,040	18.6	1.7	12,200	24.86	0.46	54.043	385	low to med.	no
57	Chauga River TL-129[c]	Brevard Zone, S.C.	--	330	21.2	640	51.8	12.5	11,000	20.21	1.12	18.045	435	low to med.	no

Table 2 con't.

58	Chauga River TL-172 [c]	Brevard Zone, S.C.	--	297	17.8	70	11.7	2.5	10,300	18.03	0.57	31.632	485	low to med.	no
59	Chauga River TL-225 [c]	Brevard Zone, S.C.	--	259	6	670	13.8	9.7	10,000	16.78	0.46	36.478	359	low to med.	no
60	Chauga River TL-486 [c]	Brevard Zone, Ga.	7	440	0	320	37	-20	26,000	9.32	1.11	8.396	523	low to med.	no
61	Chauga River C3-1 [c]	Brevard Zone, Henderson Co. N.C.	8	440	1.9	700	30	--	15,000	13.67	0.62	22.048	383	low to med.	no
62	Chauga River E1-13 [c]	BZ [e] Henderson Co., N.C.	11	440	0	820	8	--	8,300	29.22	0.34	85.94	298	low to med.	no
63	Chauga River OT-1 [c]	BZ [e] Henderson Co., N.C.	11	450	0	1,020	3	--	5,900	29.22	0.89	32.831	183	low to med.	no
64	TVA 6351-1-3	Brevard Zone, Old Fort, N.C.	--	565	6.3	165	28.0	16.9	13,200	12.75	0.75	17.00	167	low to med.	yes
65	TVA 6351-1-4	Brevard Zone, Old Fort, N.C.	--	754	10.1	300	12.0	3.3	15,300	20.36	0.23	88.522	213	low to med.	no
66	TVA 6351-1-8	Brevard Zone, Old Fort, N.C.	--	199	6.7	0	39.0	44.8	22,500	6.22	0.98	6.347	503	low to med.	no
67	Chauga River Gainesville Limestone Company	Gainesville, Ga.	--	55	4.6	130	10.8	1.9	12.300	14.45	8.32	1.737	305	low to med.	yes

[a] From field or literature data (many sources).

[b] Field sample reference number (Price).

[c] Field sample reference number (Hatcher).

[d] Field sample reference number (R. E. Lemmon).

[e] Brevard Zone.

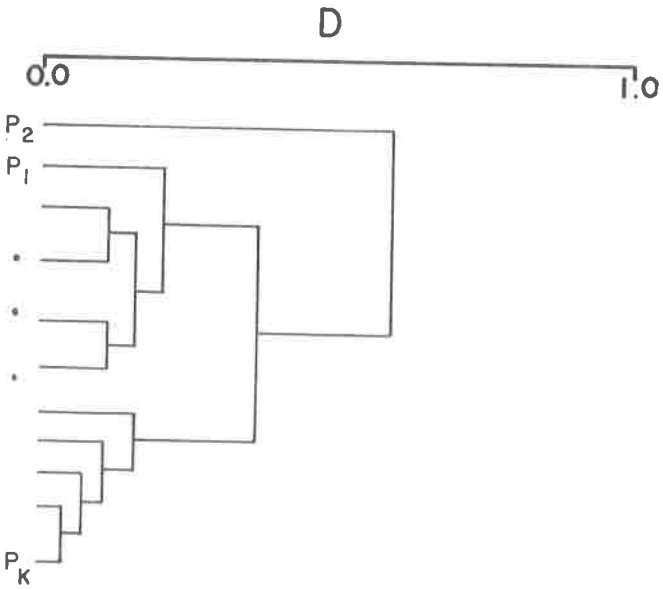

Figure 2. Cluster analysis example.

Chemical Data

Table 2 is a summary of atomic absorption and paleotemperature data used in this study. Figure 3 summarizes the average concentrations of Mn, Fe, Zn and Sr in each of the sample groups.

Certain observations may be made regarding the variation of Mn content in the different groups (Figure 3a). The Blue Ridge, Murphy, Ocoee and Chauga River samples are higher in Mn than are the others. Shady, Kings Mountain, Poor Mountain and Slice groups contain about the same average amounts. Our data do not support the contention (Rodgers, 1945) that the Shady Dolomite is characterized by its high Mn content. The mean of all samples is 440 ppm, while the high for the Shady is 440 ppm, and its mean 287 ppm.

The great variation in iron content necessitated plotting this element on a logarithmic scale. Poor Mountain, Chauga River, Blue Ridge and Ocoee samples are high in iron, averaging 10^4 ppm. As in the case of Mn, iron concentrations in Shady Dolomite and Slice samples are similar.

Chauga River, Ocoee and Slice samples are high in Zn, while Blue Ridge samples are low. Slice, Chauga River, Kings Mountain and Murphy samples are all relatively high in Sr. The Shady is low in Sr. The average Sr content of the Shady samples is 32 ppm, while the average for all samples is 271 ppm. This may reflect a chemical characteristic of dolomites.

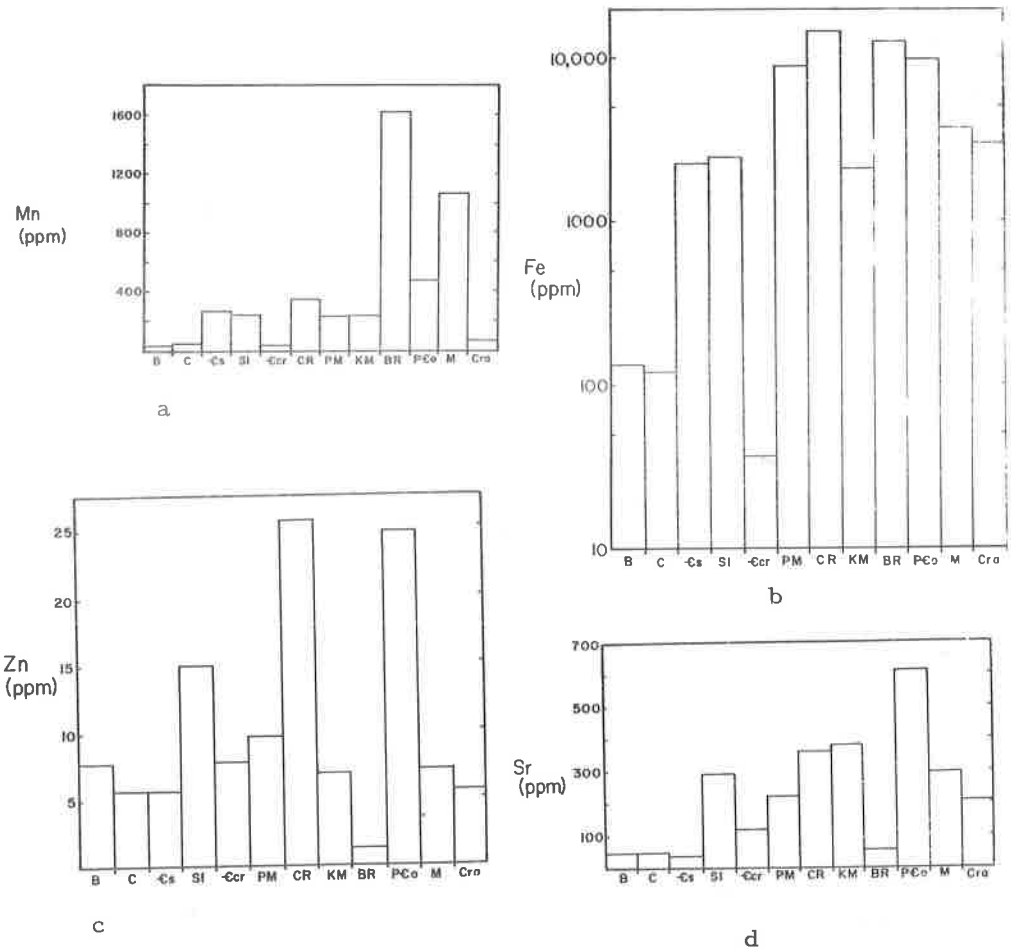

Figure 3. Average concentrations of Mn(3a), Fe(3b), Zn(3c) and Sr(3d) in the sample groups. B - Bandana marble (Dolomite, Blue Ridge, North Carolina). C - Chewacla Marble (Dolomite, Pine Mountain Belt, Alabama. Cs - Shady Dolomite. Sl - Tectonic slice material from the Brevard fault zone. Ccr - Copper Ridge Dolomite. CR - Chauga River Formation. PM - Poor Mountain Formation. KM - Kings Mountain belt samples. BR - Blue Ridge. PCo - Ocoee Supergroup carbonates. M - Murphy belt carbonates (Murphy marble). Cra - samples from various localities in the craton.

Paleotemperatures

Samples from the western Blue Ridge and Valley and Ridge record low temperatures as would be expected (270° or less). Murphy samples yield an average temperature of about 360°, which is consistent with the observed occurrence of talc, tremolite - actinolite and

staurolite in these rocks (Hurst, 1955; Power and Forrest, 1971). Manley and Power (1972) report somewhat higher temperatures for the Murphy belt.

Southeastward certain anomalous temperatures were determined. The temperature of the Chauga River carbonates varies along strike, reaching over 600° in South Carolina and decreasing to about 400° to the southwest. To the northeast it decreases to about 300°. The progressive regional metamorphic grade is garnet to staurolite, subsequently retrograded to chlorite. The higher Chauga River temperatures are greater than would be expected even if these carbonates equilibrated at the peak progressive metamorphic temperature. Tectonic slice samples yield a maximum of 320°C and average about 250°. We attribute the high Chauga River temperatures to short-term frictional heating during deep-seated Brevard faulting. The slices were picked off later from the footwall at a shallow depth and consequently were not subjected to extreme frictional heating (see Hatcher, 1971, Figure 8).

Poor Mountain carbonates average about 340°C which is consistent with the regional metamorphic grade. Kings Mountain Belt samples yield temperatures lower than the progressive regional metamorphic grade.

The Mg/Ca ratios as determined by atomic absorption versus the measured paleotemperatures are presented in Figure 4. Samples which have Mg/Ca ratios well above the solvus should record temperatures which are not limited by Mg deficiency. Samples immediately above the solvus may contain dolomite in amounts less than the limit of detection by X-ray diffraction (approximately 5 percent). Samples which plot on the solvus probably contain no dolomite and thus because of Mg deficiency yield temperatures which are too low. Such temperatures are still useful since they provide a minimum temperature for a thermal event.

Cluster Analysis

Cluster analyses were performed on various combinations of samples and variables. The results of two of these analyses are presented in Figures 5 and 6. Some general trends which recur in several of the analyses are exemplified by Figure 5. The best defined groups are: (1) the dolomite group consisting of all Shady samples plus several other dolomites. (2) A group consisting of dominantly calcitic rocks which includes all our Kings Mountain samples plus five other samples. (3) A group containing nearly all the Chauga River samples plus one Ocoee, one Blue Ridge and one Murphy. Chauga River samples are consistently split into two sub-groups in every cluster analysis regardless of the number or combination of variables chosen. (4) A group composed of representatives of several different lithologies, principally Murphy and Poor Mountain. We do not know why they cluster in this way. (5) A group dominated by the slice samples which contain both

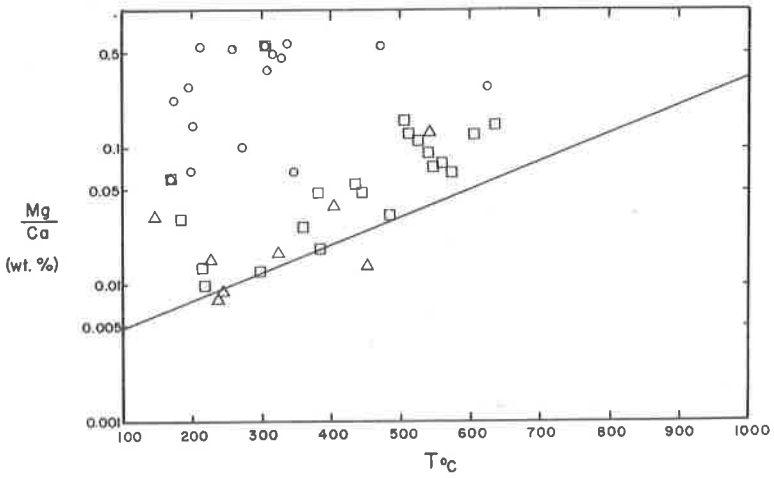

Figure 4. Plot of Mg/Ca vs. temperature. The solid line is the magnesian calcite solvus plotted from the data of Graf and Goldsmith (1958) and Goldsmith and Newton (1969). The squares represent Chauga River Formation samples. The circles represent non-Chauga River samples containing both calcite and dolomite. The triangles represent dolomite-free non-Chauga River samples. The two squares containing a circle represent Chauga River samples containing dolomite.

calcite and dolomite. The fact that the slice samples do not cluster with the main dolomite group (mostly Shady samples) may indicate that the slice rocks probably are not Shady as previously interpreted by Hatcher (1971). The presence of a Copper Ridge sample with slice samples in this and other cluster diagrams may be significant. The one Chauga River sample clustered with the slices may indeed be a tectonic slice.

Figure 6 is a cluster diagram based on variables chosen to minimize groupings on gross mineralogy. The primary criterion for choosing these elements is that they had low correlation coefficients with Ca and Mg and with one another. Note that two Chauga River groups are still distinct. Shady samples which previously were confined to an all dolomite group are now dispersed. Even in this diagram tectonic slices show no affiliation with Shady samples.

CONCLUSIONS

1. Each lithologic unit exhibits a characteristic range of paleotemperatures and elemental concentrations. Most sampled units seem

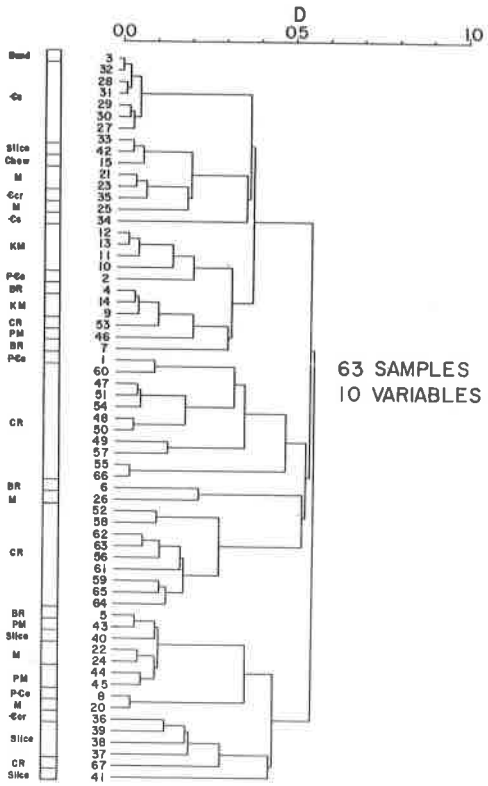

Figure 5. Representative cluster diagram. D-distance function. Band-Bandana marble. Chew-Chewacla marble. See caption to Figure 3 for explanation of other symbols. The numbers are sample numbers in Table 1.

to be internally consistent and, at this stage of our study, no definite large scale cross unit correlations have been made. A tentative correlation is suggested by the fact that the Black Mountain, North Carolina Ocoee sample is clustered with the Chauga River samples.

2. We believe that an unknown sample from one of the groups of rocks studied could be assigned to its proper group utilizing the techniques of this study.

3. In the Chauga River group, where sampling is felt to be adequate, we see consistent patterns of clustering which can be related to field or petrographic observations. The high Chauga River temperatures, which exceed 500°C in many samples, are attributed to short-term frictional heating during deep seated Brevard faulting which post

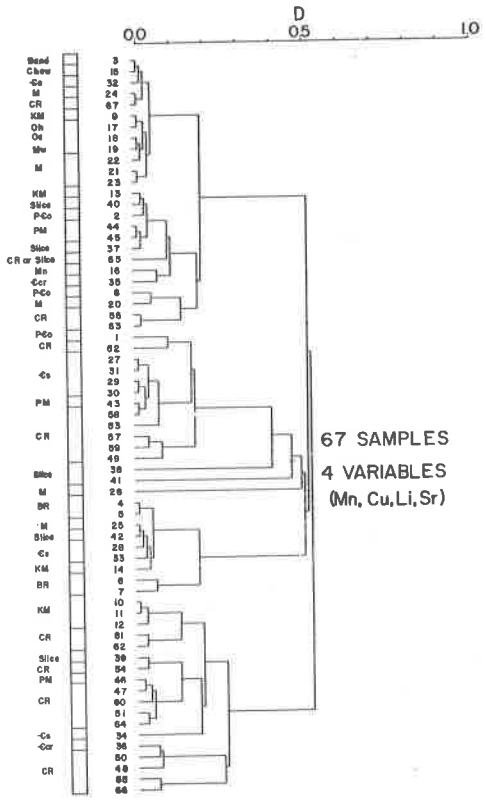

Figure 6. Cluster analysis diagram of four elements. See Figures 3 and 5 for explanation of symbols.

dated regional metamorphism.

4. The influence of gross mineralogy on groupings can be minimized by proper choice of variables, as seen in Figure 6.

REFERENCES CITED

Goldsmith, J. R., Graf, D. L., and Joensuu, O. I., 1955, The occurrence of magnesian calcites in nature: Geochim. et Cosmochim. Acta, v. 7, p. 212-230.

Goldsmith, J. R., and Newton, R. C., 1969, P-T-X relations in the system $CaCO_3$-$MgCO_3$ at high temperatures and pressures: Am. Jour. Sci., v. 267-A, p. 160-190.

Graf, D. L., and Goldsmith, J. R., 1958, The solid solubility of $MgCO_3$

in $CaCO_3$: a revision: Geochim. et Cosmochim Acta, v. 13, p. 218-219.

Hatcher, R. D., Jr., 1969, Stratigraphy, petrology, and structure of the Low Rank Belt and part of the Blue Ridge of Northwesternmost South Carolina: South Carolina Devel. Board Div. Geology, Geol. Notes, v. 13, p. 105-141.

_____, 1971, Stratigraphic, petrologic and structural evidence favoring a thrust solution to the Brevard problem: Am. Jour. Sci., v. 270, p. 177-202.

Hurst, V. J., 1955, Stratigraphy, structure and mineral resources of the Mineral Bluff Quadrangle, Georgia: Georgia Geol. Survey Bull. 63, 137 p.

Manley, F. H., and Power, W. R., 1972, Calcite thermometry in the Georgia Piedmont (abs.): Geol. Soc. America Abstracts with Programs, v. 4, p. 89.

Parks, J. M., 1966, Cluster analysis applied to multivariate geologic problems: Jour. Geology, v. 74, p. 703-715.

Power, W. Z., and Forrest, J. T., 1971, Stratigraphy and structure of the Murphy belt, North Carolina: Carolina Geol. Soc. Guidebook, 29 p.

Snipes, D. S., in preparation, Regression functions relating the d-spacing, composition and equilibration temperatures of magnesian calcite: unpublished manuscript, 20 p.

Rodgers, John, 1945, Manganese content of the Shady Dolomite in Bumpass Cove, Tennessee: Econ. Geology, v. 40, p. 129-135.

MESSELITE AT KINGS MOUNTAIN, NORTH CAROLINA

By

Donald R. Privett
Department of Geology
Catawba College
Salisbury, North Carolina 28144

ABSTRACT

Messelite (Ca, Fe, Mn, Mg)$_3$ (PO4)$_2$2. O H_2O, in hemispherical crystal aggregates (1-3mm), has been identified for the first time as occurring in spodumene pegmatite fractures at the Foote Mine, Kings Mountain, North Carolina. The messelite probably crystallized from late stage phosphate rich solutions moving in the cooling fractures of the pegmatites. X-ray, D. T. A., chemical and optical data are presented. The messelite from Kings Mountain, except for the somewhat higher Mn content, is similar to messelite reported from the four other known occurrences.

INTRODUCTION

Messelite, (Ca, Fe, Mn, Mg)$_3$ (PO$_4$)$_2$ 2. O H_2O is present in fractures of the spodumene pegmatites exposed at the Foote Mineral Company mine at Kings Mountain, Cleveland County, North Carolina. The purpose of this note is to present optical, D. T. A. chemical and x-ray data for the mineral at this occurrence.

The geology of the Kings Mountain belt and the Foote Mine was described by Kesler (1961). Thin layered amphibolites and muscovite schists are intruded by a swarm of spodumene pegmatites. The pegmatites consist of pairs and clusters of tabular dikes. At the mine, the largest dikes are 330 m long by 66 m thick; however most are only 6-33 m thick. They strike NNE and dip steeply east and west. The pegmatites are uniform in composition, containing 41 percent feldspar, 32 percent quartz, 20 percent spodumene, 6 percent muscovite, and 1 percent accessory and secondary minerals.

The area is quickly becoming unique in regard to the number of unusual late stage hydrothermal and secondary minerals present in fractures of the pegmatites. White (1969) has identified over 80 different minerals from within the quarry.

Recently, two new minerals, switzerite (Leavens and White, 1967) and eakerite (Leavens, White and Hey, 1970), and three rare minerals; eucryptite and bikitaite (Leavens, Hurlbut, and Nelen, 1968) and lithiophosphate (White, 1969) have been described.

Messelite was originally named and described by Muthmann (1890) for material from Messel in Hesse, Germany. Wolfe (1940) studied material from the same area and considered messelite to be a mixture of anapaite and questionable collinsite and thus not a valid species. Frondel (1955) described material from Palermo, New Hampshire, having the composition of the original messelite, but called it neomesselite - $(Ca, Fe, Mn, Mg)_3 (PO_4)_2 \; 2 \; H_2O$ - and iron-rich analogue, isostructural with fairfieldite. He considered anapaite (messelite) to be a crystallographically distinct higher hydrate, isostructural with papahopeite. Re-study of material from Hesse by Cech and Padera (1958) showed it to be identical to the neomesselite of Frondel. Neomesselite should therefore be discarded as a mineral name (Cech and Padera, 1958, Fleischer, 1959) since the original material studied and defined by Muthmann contained predominately messelite. The only other reported occurrences of messelite are in Kazakstan, U. S. S. R. and in Czechoslovakia.

Acknowledgments

I am indebted to O. C. Kopp, Department of Geology, University of Tennessee, for performing the D. T. A. analysis. A. Antonakos was very helpful in securing funds for the chemical analysis from the faculty research grant of Catawba College.

PHYSICAL AND OPTICAL PROPERTIES OF MESSELITE

Messelite at Kings Mountain is present as radiating hemishperical to globular crystal aggregates 1-3 mm in diameter, coating some fracture surfaces of the spodumene pegmatite. The hemispheres are composed of tiny radiating, interpenetrating crystals. Some hemispheres are solid; however most contain a void at the center. A distinct cleavage in two directions is apparent in finely crushed material. Indices of $\eta\alpha$ = 1.644 (4) $\eta\beta$ = 1.653, $\eta\gamma$ = 1.660 were obtained. The messelite is biaxial positive, and has low birefingence, $2V=30^{o}$, extinction angle $35\text{-}54^{o}$. Incomplete extinction was observed in almost all grains, this was also noted by Wolf (1940).

X-RAY DIFFRACTION

Table 1 shows the x-ray powder diffraction data for messelite from Kings Mountain and neomesselite from Palermo, New Hampshire (Frondel, 1955). The data for the Kings Mountain messelite is the average for five different samples. The x-ray data for both materials are very similar except for the absence of reflections at 9.00Å or 7.01Å, 3.49Å, 2.48Å, 2.25Å, and 2.05Å in the Kings Mountain material. Cech

Table 1. X-ray Powder Diffraction Data for Messelite.

Kings Mountain[a] d(obs)Å	I/I$_o$	Palermo, N. H.[b] d(obs)Å	I/I$_o$	Kings Mountain[a] d(obs)Å	I/I$_o$	Palermo, N. H.[b] d(obs)Å	I/I$_o$
		9.00	3			2.48	3
		7.01	3	2.45	1	2.45	3
6.36	10	6.34	10	2.41	1	2.41	2
5.07	2	5.07	6	2.35	2	2.35	3
4.57	1	4.57	4			2.25	1
4.50	2	4.51	4	2.23	1	2.23	3
3.84	1	3.83	4	2.21	1	2.21	1
3.75	1	3.74	4	2.12	2	2.13	4
3.58	3	3.58	4	2.10	2	2.10	4
		3.49	3			2.05	1
3.37	1	3.40	2	2.00	1	2.02	3
3.34	1	3.34	2	1.99	1	1.989	1
3.28	2	3.28	6	1.96	1	1.962	3
3.17	10	3.17	10	1.93	1	1.923	1
3.02	9	3.02	8	1.878	1	1.875	2
2.95	1	2.95	3	1.840	1	1.839	4
2.88	2	2.86	4	1.809	1	1.813	4
2.80	3	2.79	6	1.791	3	1.788	7
2.67	6	2.68	8	1.710	3	1.708	6
2.63	3	2.62	4	1.687	2	1.689	6
2.57	3	2.57	7	1.659	1	1.656	4

a average of 5 separate analyses, Diffractometer Ni-filtered CuKα radiation, 30Kv, 15 ma, 1°-2θ per minute, 1° divergence slit, 0.01 inch receiving slit.

b Frondel, 1955, data for "neomesselite." p. 831.

and Padera (1958) did not detect reflections at 9.00Å or 7.01Å in their analysis of the Palmero material. The other reflections may be ascribed to an additional component in the Palermo material, which is not present in the messelite from Kings Mountain.

Frondel mentions the presence of parallel needle-like inclusions. The material from Kings Mountain is optically homogeneous.

THERMAL STUDY

D. T. A. analysis of messelite is characterized by endothermic peaks at 385±5°C (strong) and 440±5°C (weak) that represents the loss of free water; a weak exothermic peak at 680±5°C is also present. The samples (0.05g) were ground to -50 mesh and run using alumina as inert material. The curve was obtained on both 33,000x and 10,000x amplification at 12°C per minute.

Table 2. Chemical Analyses of Messelite.

	1	2	3	4	5	6
CaO	25.64	23.19	28.00	27.08	29.47	30.02
MgO	0.09	1.36	0.77	1.19	2.97	
FeO	16.62	21.75	11.54	18.17	17.27	3.42
MnO	7.87	3.94	7.35	0.12		17.40
P_2O_5	38.96	36.90		38.99	38.75	37.69
H_2O	11.00	11.30		12.92	10.89	9.70
Insol		1.39		1.71	0.87	1.66
Total	100.18	99.83		100.18	100.22	100.00

1. Messelite. Kings Mountain, N. C. This study. K. V. Rodgers, Analyst, Southwestern Analytical Laboratories.
2. "Neomesselite." Palermo, N. H. Greenish white granular. Frondel, 1955, p. 830.
3. "Neomesselite." Palermo, N. H. White, platy-fiberous. Frondel, 1955, p. 830.
4. Messelite. Kazakstan, U. S. S. R. Cech and Padera, 1958, p. 447.
5. Messelite. Messel in Hesse, Germany. Wolfe, 1940, p. 791.
6. Fairfieldite. Branchville, Conn. Palache, Berman, and Frondel, 1963, p. 721.

CHEMICAL COMPOSITION

A chemical analysis of 46 mg of messelite picked from a sample under the binocular microscope, is presented in Table 2. Four additional previously published analyses of messelite and one of fairfieldite, from other reported occurrences are presented for comparison.

Messelite from Kings Mountain is enriched in Mn and low in Mg and is, except for the lower Mg and Fe, very similar in composition to the "neomesselite" described by Frondel (1955). From the tabulated analyses it is apparent that Mg, Mn, and Fe can vary fairly widely; this analysis, therefore, helps to substantiate that messelite forms a solid solution series with fairfieldite (Frondel, 1955). Fairfieldite contains less FeO and more MnO than messelite.

CONCLUSIONS

The fifth known occurrence of messelite is reported. It occurs as hemispherical crystal clusters in shrinkage fractures of the spodumene pegmatites exposed at Kings Mountain, North Carolina, having

crystallized from late stage phosphate-rich hydrothermal solutions. When compared with published chemical data from three of the four other known occurrences, the Kings Mountain messelite is enriched in Mn and low in Mg and constitutes part of a solid solution series with fairfieldite.

REFERENCES CITED

Cech, F., and Padera, K., 1958, Messelit aus den Phosphatnestern im Granit bei Pribyslavice (Böhmen) und das Messelitproblem: Chem. der Erde: v. 19, p. 436-449.

Fleischer, M., 1959, New Data: Am. Min., v. 44, p. 469.

Frondel, C., 1955, Neomesselite and Beta-roselite: Two new members of the Fairfieldite Group: Am. Min., v. 40, p. 828-833.

Kesler, T. L., 1961, Exploration of the Kings Mountain pegmatites: Min. Eng., v. 13, p. 1062-1068.

Leavens, P. B., Hurlbut, C. S., Jr., and Nelen, J. S., 1968, Eucryptite and bikitaite from Kings Mountain, N. C.: Am. Min., v. 53, p. 1202-1207.

Leavens, P. B., and White, J. S., Jr., 1967, Switzerite $(Mn, Fe)_3(PO_4)_2 \cdot 4H_2O$, a new mineral: Am. Min., v. 52, p. 1595-1602.

Leavens, P. B., White, J. S., Jr., and Hey, M. H., 1970, Eakerite - a new tin silicate: Mineralogical Record, v. 1, p. 92-98.

Muthman, W., 1890, Messelit, ein neues mineral: Zeit. Krist., v. 17, p. 93-94.

Palache, C., Berman, H., and Frondel, C., 1963, Dana's System of Mineralogy: v. 2, seventh edition, John Wiley, and Sons, p. 720.

White, J. S., Jr., 1969, A lithiophosphate occurrence in North Carolina: Am. Min., v. 54, p. 1467-1469.

Wolfe, G. W., 1940, Classification of minerals of the type $A_2(XO_4)_2 nH_2O$: Am. Min., v. 25, p. 738-753.

PATTERNS OF SEDIMENT TRANSPORT AT NEARSHORE ZONES INFLUENCED BY WAVE AND TIDAL CURRENTS: A STUDY UTILIZING FLUORESCENT TRACERS

By

George F. Oertel
Skidaway Institute of Oceanography
P. O. Box 13687
Savannah, Georgia 31406

ABSTRACT

In nearshore zones, responses of detritus to moving water illustrate several different transportational and depositional patterns depending on the nature of the interactions between wave surge and tidal flow. The concept of flow regime as applied to fluvial environments is not completely applicable in zones exhibiting these interactions. Turbulent wave processes are also not completely suitable for explaining the orientations, textures and structures of the bedforms in these zones. The resultant force produced by the interaction of wave surge and tidal currents may have a greater influence on sedimentation than these individual components. Studies using fluorescent-tagged grains proved to be a valuable method for analyzing sedimentary responses to the complicated interactions of wave surge and tidal flow.

At offshore, shallow, subtidal areas the greatest distances of sediment transport generally correspond to the direction of tidal flow, while bedform configurations are predominantly effected by wave surges. At offshore intertidal areas, bedform configurations and the greatest distances of sediment transport are largely controlled by surging waves. During the flooding tide, the approach directions of surging waves determine the bedform configurations and the greatest distances of sediment transport. When wave surge and tidal currents are in opposing directions (during the ebbing tide), sediment is entrained in gyral paths. These sediment gyres cause deposition of sand in the horizontal strata of planar beds.

At the shorelines adjacent to the estuary entrances, tidal currents and wave currents are in mutually evasive zones and patterns of sediment entrainment generally conform to the directions of the water flow in the respective zones. When tidal currents and longshore currents are in opposite directions, then the entrainment of sediment corresponds to the bi-polar flow directions in the respective current zones.

INTRODUCTION

Wave refraction around seaward extending shoals results in a concentration of wave energy at shoals, which generally causes headland erosion and the landward displacements of a portion of the shoals. However, in some nearshore areas the interactions of wave surge with river flow and tidal currents produce concentrations of sand which nourish the shoals and inhibit the erosional effects of wave attack (Oertel and Howard, 1972; Oertel, 1972). Different combinations of wave and current interactions cause complicated patterns of grain transport that are not always reflected by the bedform configurations. In these areas, the use of bedforms for current and sediment transport analysis is restricted.

Sand shoals illustrating complicated patterns of sediment transport are present in large numbers along the mesotidal shorelines (Hayes, 1972) of the Georgia coast. The shoreface adjacent to the south end of Sapelo Island has an undulating sand-shoal surface that is exposed to multi-directional tidal currents and shoaling waves. The interactions between the forces of shoaling waves and tidal currents result in flow characteristics that differ from the characteristics of fluvial flow-regimes (Simons, Richardson, Nordin, 1965; Harms and Fahnestock, 1965), and the concepts of flow regimes are invalid at these portions of the nearshore zone.

Patterns of wave refraction and multi-directional tidal flow are important parameters controlling the locations and configurations of nearshore sand banks (Tanner, 1960; Robinson, 1966; Oertel and Howard, 1972). Numerous combinations of wave-surge/tidal-current interactions are possible because the directions of tidal flow are bi-polar and the directions of wave surge are continually changing as wave-crests refract, wrap around and interfer at shoals. The transportational and depositional responses of detritus to these interactions are very complicated and difficult to evaluate. However, techniques utilizing fluorescent-tagged grains are ideally suited for tracing complex patterns of sand dispersion. During the summer of 1970, patterns of sand transport were studied at intertidal portions of the ramp-margin shoals at the south end of Sapelo Island, Georgia. Studies were done by using grain-tracing techniques modified after Jolliffe (1963) and Ingle (1966). In 1963, Jolliffe conducted a study using tagged grains to trace trends of sand movements on an offshore sand bank at the entrance to Lowestoft Harbor. The grid he used permitted a moderately long term evaluation (21 days) of the sediment exchange between various parts of a subtidal sand bank and the beach; however, the stations were placed too far apart to permit an analysis of the local transport patterns responding to the various interactions between wave surge and tidal currents. In the present study, a grid with closely spaced sample stations (25 feet) was used to study patterns of sand dispersion in response to these interactions.

Acknowledgments

The field work for this study was assisted by S. A. Greer, J. B. Kirchoffer and G. H. Remmer. I would also like to thank my secretary, J. Davis, for typing the manuscript. This study was partially supported by the U. S. Corps of Engineers contract DACW 72-68-C-0030 and NSF Grant GA-30565. J. D. Howard was the principal investigator of these grants.

PROCEDURE

Four sample grids were established on the sand bed of the nearshore zone at the following depths relative to low water: 1) at a subtidal surface of an offshore sand shoal exposed to the residual wave-surge (Swift, 1969), 2) at a subtidal surface of an offshore sand shoal shielded from the effects of residual wave-surge, 3) at an intertidal surface of an offshore sand shoal exposed to interfering wave crests, 4) at an intertidal surface of the foreshore zone with mutually evasive zones of tidal currents and wave-induced currents. Sand taken from the sea bed at these sites was coated with fluorescent paints. The painted sand was color coded for the four different grids and for the ebb and flood sampling periods. Tagged grains were released on the sand bed at the upcurrent (tidal current) and of the respective sample grids and samples were collected after relatively short intervals of water-sediment interaction. Sampling was conducted during ebb and flood sampling periods when maximum tidal current velocities over the sand-shoal surfaces varied from 50 to 70 cm/s. Patterns of wave refraction and tidal flow were recorded in conjunction with tracer sampling. At each station a 100 sq cm surface sample was taken with a vaseline covered card. Samples were analyzed in the laboratory to determine the amount of fluorescent sand at each station, and these data were plotted on base maps of the sample grid. From these maps, patterns of dispersion and sedimentation were determined.

DISCUSSION OF DISPERSION PATTERNS

In areas having complex patterns of wave refraction, it has been noted that bedforms may not reflect the local directions of wave surge (Tanner, 1960) or the local directions of tidal flow (Oertel, 1969). Quite often a variety of orientations is exhibited by bedforms in these areas and some of these orientations cannot be attributed to any of the obvious forces. The resultant force produced by the interaction of wave surge and tidal currents often has a greater influence on sedimentation than any of the component forces focusing on sea-bed surfaces. In many cases, the last force active above the sea bed prior to deposition is the

most influential in molding bedforms (Oertel, 1969). Hence, bedform orientations at these tidal environments, are not suitable for use as indicators of the predominant direction of tidal flow or sediment transport. The dispersion patterns of tagged-grains at these environments appear to illustrate the relationship between bedforms, directions of sediment transport, and complex interactions between wave surge and tidal flow.

Subtidal Surfaces of Offshore Sand Shoals Shielded from Wave Surge

In subtidal areas exposed to multi-directional tidal flow, but shielded from onshore wave-surge, the flow of tidal currents over the sand bed produced regularly spaced dunes that are characteristic of lower flow-regimes (Simons, Richardson, and Nordin, 1965; Harms and Fahnestock, 1965). Since wave-surge was shielded from the sample grid by sand ridges, patterns of dispersion for ebbing and flooding currents were very similar, although directions of transport were approximately opposite for the ebbing and flooding periods. Dunes on the sand bed were in the megaripple size-range and had short (2 m) cuspate or linguiodal crests (Figure 1a). However, isopleth patterns of tagged grains did not appear to be related to the shapes and configurations of the dunes on the bed. Grain concentrations decreased away from the release points and trends of isopleths were parallel to the directions of tidal flow (Figure 1b). Evidently, rates of grain burial and grain re-exposure at the sand bed were essentially equal, resulting in a regular decrease in grain concentrations away from the release points.

Subtidal Surfaces of Offshore Sand Shoals Exposed to Wave Surge

Sand dispersion was studied on a portion of the sea bed that was one meter below the intertidal zone of a longshore trending shoal and exposed to the onshore surge of waves. The sea bed at the sample grid was an undulating surface covered with large and small dunes illustrating a variety of orientations. In these areas, residual onshore wave-surge may be produced by waves with periods greater than six seconds or waves having relative heights (wave height/water depth) greater than 0.2-0.4 (Inman and Nasu, 1956, Swift, 1969). The relative wave heights at this study area fit into this category and generally resulted in a time-velocity assymetry of wave surge (Swift, 1969) capable of producing a residual onshore surge. During the flooding tide, the directions of tidal flow and wave surge were both onshore. However, tidal flow was toward an inlet and tended to be oblique to the beach and to the southwest. Wave crests that were moving landward were elevated above the still-water level as they surged over shoal surfaces. The refraction of waves in this area tended to orient wave crests parallel to the shoal trend and since the shoal was elongate in a longshore rather than offshore direction, wave crests generally did not interfere over the shoal surface.

a.

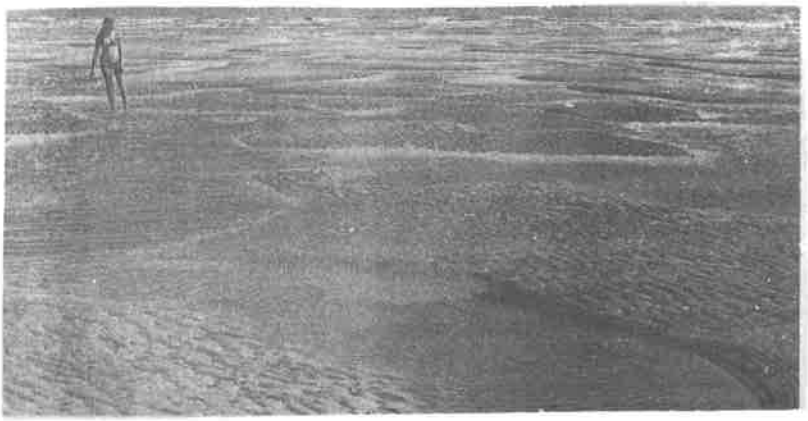

b.

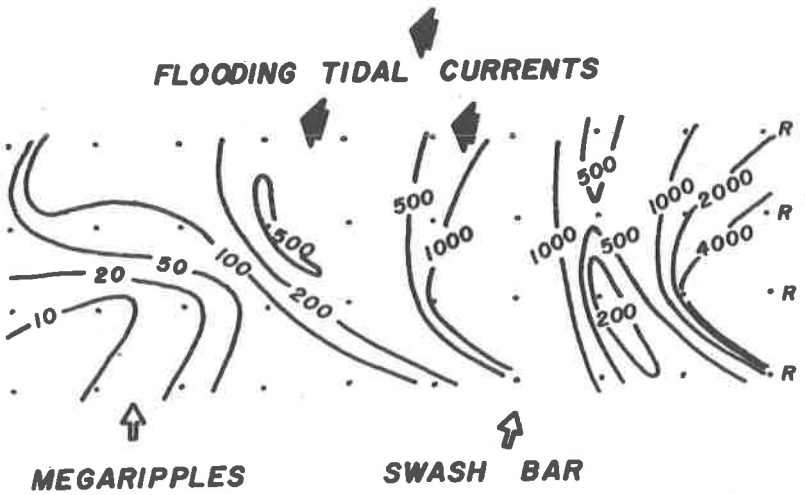

Figure 1(a) Surface of a sand shoal exposed during spring low tide. This area is bathymetrically shielded from wave surge by a swash bar. Cuspate and linguiodal megaripples are present on the sediment surface. The figure in the photo is approximately 1.75 meters in elevation. (Photo from Oertel, 1971). (b) Map of a sample grid in the area shown in Figure 1a. Isopleth contours illustrate the dispersion pattern of fluorescent-tagged sand during the flooding tide. Fluorescent-tagged sand was released at points R in a 50-70 cm/s flooding current and collected at stations indicated as dots on the grid. Collection was standardized to a time approximately 10 minutes after release. Isopleth contours represent the number of fluorescent-tagged grains recovered per 100 sq cm.

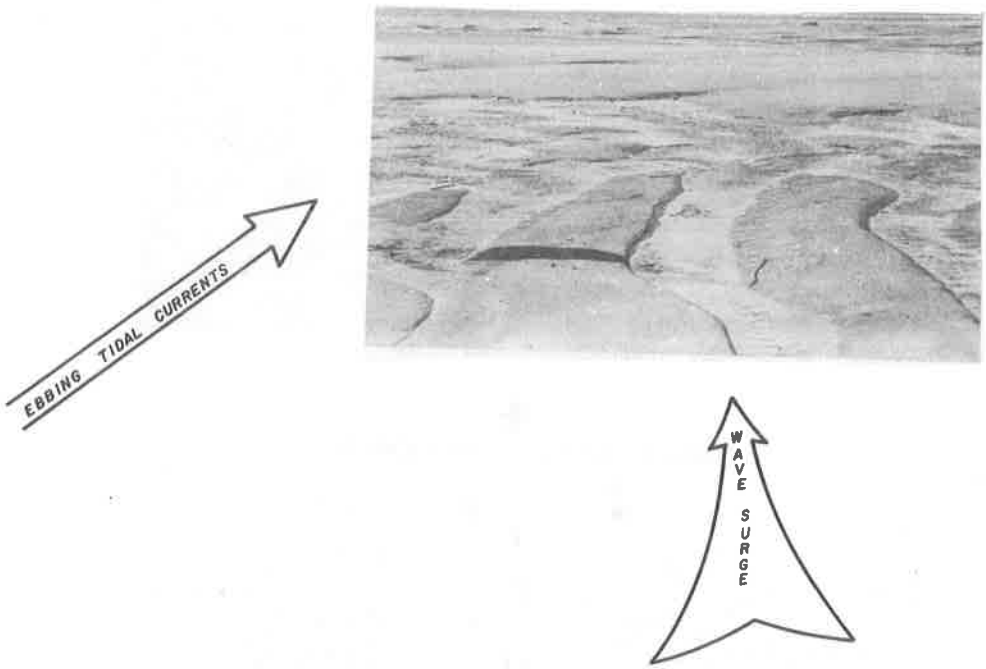

Figure 2. Photo illustrating the relationship of flat-crested megaripples with wave and tidal currents on the margin of an offshore trending shoal. Megaripples have 5 to 6 foot wave lengths and are located in the subtidal areas, but are exposed during spring low tide. The planar surface of a swash platform is discernible behind these flat-crested dunes.

The irregular dispersion patterns of tagged grains released on this surface were probably the result of differential rates of burial at dune crests and dune troughs. Local concentration trends of tagged grains formed parallel to the long axis of large (up to 20 foot wave lengths), flat and linear crested dunes (Figure 3a, 3c). The steep faces of these dunes were generally oriented oblique to tidal flow, and the long axis tended to be parallel to the direction of wave surge (Figure 2, 3b). The longest distance of sand transport at the sample grid corresponded to the direction of tidal flow, however, the direction of tidal flow did not correspond to the slip faces of the dunes.

During the ebbing tide, the directions of tidal flow and wave surge were approximately normal to each other. Wave surge was directly onshore while tidal flow was offshore at an oblique angle with the beach (Figure 3c). The longest distance of grain dispersion was

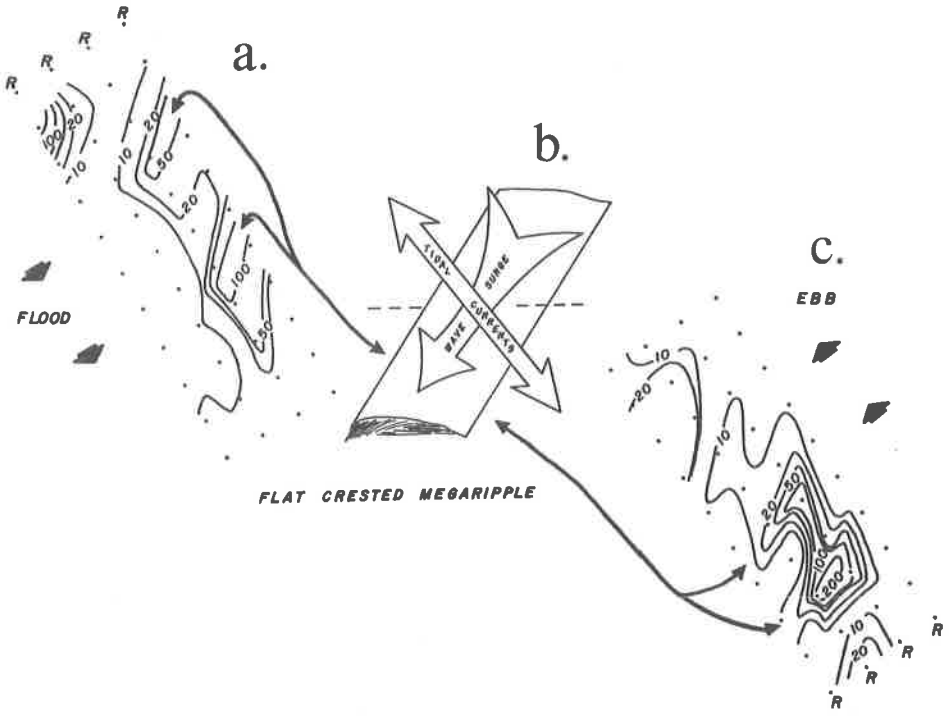

Figure 3(a). Isopleth map located at a portion of longshore trending sand shoal that was influenced by the surge of shoaling waves. Isopleth contours illustrate the dispersion pattern of sand during the flooding tide. Isopleths outline the shape of large, flat-crested megaripples. The direction of the greatest distance of grain transport is parallel to the direction of flooding tidal currents. Concentrations are in grains per 100 sq. cm. (R) designates the release points of tagged sand. (b) Sketch of a flat-crested megaripple illustrating its orientation with respect to wave surge and tidal flow. (c) Isopleth map of a sample grid analyzed during the ebbing tide, and in an area influenced by the surge of shoaling waves. Tracer isopleths outline the shape of large flat-crested megaripples but illustrate that the direction of ebbing tidal currents corresponds to the direction of the greatest distance of grain transport. Concentrations are in grains of 100 sq. cm. (R) designates release points of tagged sand.

offshore and corresponded to the direction of ebbing tidal currents, however, the tagged-grain concentration at the down-current end of the ebb sample-grid was approximately half the concentration found at the down-current end of the grid during the flood sample period. During the ebbing tide, tagged grain concentrations formed isopleth lines that were

parallel to directions of wave surge. The orientation of the bedforms appears to be more closely related to the direction of surging waves than to the direction of tidal flow. Hence, observations of the sample grids indicate that where shoaling waves were elevated above the still water level, (but not to the point of breaking) as they surge across shallow parts of sand banks, the surge of waves appeared to flatten and orient bedforms although the tidal currents appeared to transport sediments the greatest distances.

Intertidal Surface of Offshore Sand Shoals Exposed to Refracted and Surging Waves

Sand-dispersion analysis was conducted at a sand shoal trending offshore that was exposed to bi-directional tidal flow and interfering wave crests. Although tidal currents were the dominant force transporting sand toward intertidal surfaces of shoals, the forces of refracted waves controlled the patterns of sand dispersion once the sediment had arrived at the surfaces of the sand shoals. During the ebbing tide, the directions of wave surge and tidal flow were at oblique angles to each other, and wave refraction produced three directions of wave surge that advanced across shoal surfaces (Figure 4a, b). Refraction caused wave crests to wrap around shoals and produce surges of water advancing onto the shoals in two onshore directions. A third onshore direction of wave surge was produced along the points of interference between these two refracted wavecrests (Figure 4a, b). The force of this third surge was generally the strongest of the three forces and was frequently accented by a wave bore at the point of interference. Tidal currents crossed the intertidal portions of the sand shoals at oblique angles and interacted with the three directions of wave surge (Figure 5a). During a tidal cycle, the three directions of wave surge generally remained relatively constant whereas the tidal flow reversed directions during the ebbing and flooding tides. As a result of these tidal-current reversals, the characteristics of the interactions between wave surge and tidal currents were different as were the transportational responses of sediment to these interactions.

During the ebbing tide, tagged grains (that entered the upcurrent and landward end of the sample grid) were transported seaward onto the intertidal surfaces of the sand shoals by tidal currents. Upon reaching these areas, sediment was immediately reworked and transported landward by surges of water associated with refracted and interfering wave-crests (Figure 5b). The initial seaward transport of sediment followed by a landward return of that sediment, produced a gyral flow of sediment over the shallow portions of shoals. These sediment gyres produced relatively high rates of deposition that may result in a net accumulation of sediment. Below the gyral flow of sediment, surfaces were planar, whereas, the sand bed outside of this interaction zone was

a.

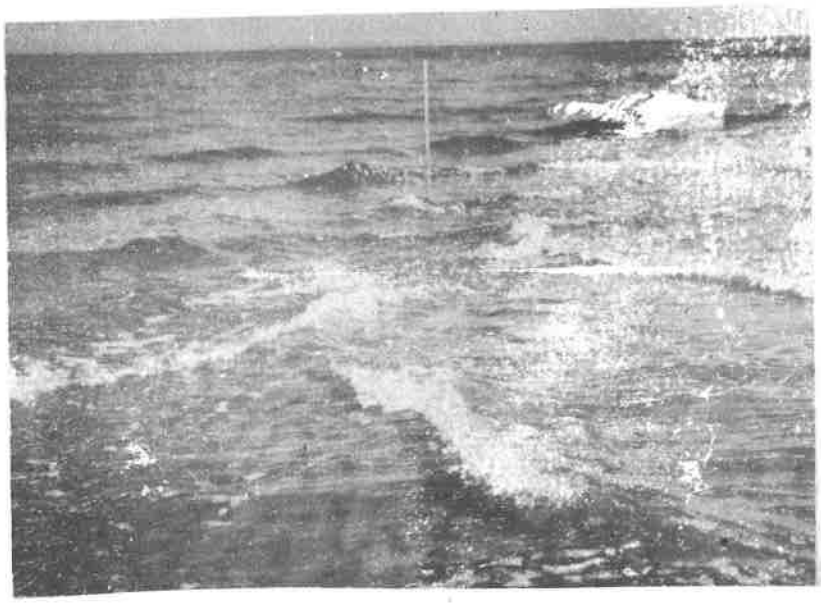

b.

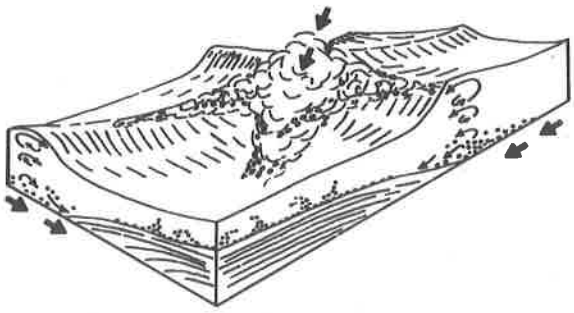

Figure 4(a) Photo of wave refraction on seaward extending sand shoal (from Oertel, 1968). Wave crests interfere along the axis and the highest portion of the sand body. Flat-crested ripples on the sand bed are parallel to a line bisecting the angle between the refracted wave-crests. (b) Sketch of a bore produced by interfering wave crests. The black arrows illustrate the three different approach directions of surging waves.

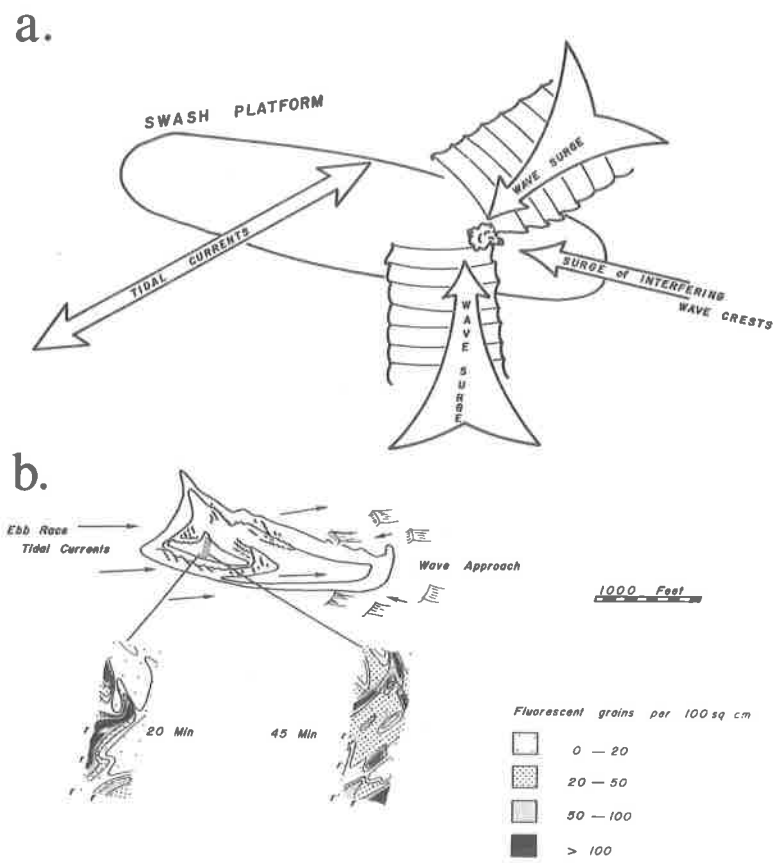

Figure 5(a) Sketch map of a swash platform (oriented onshore-offshore) on a sand shoal. Arrows indicate the nature of the currents interacting above the axis of the swash platform. (b) Map of sand shoal and a tagged-grain sampling grid. Isopleths record the pattern of grain transport during the ebbing tide. Sediment gyres that result from wave-surge/tidal-current interactions produce curved isopleth patterns. (r) designates release points of tagged sand. (Adopted from Oertel, 1972).

generally covered by megaripples.

During the flooding tide, directions of wave surge and tidal flow were all onshore, however, refraction did produce some wave-surge/tidal-flow interactions although not to the magnitude found during the ebbing tide. The turbulent surges produced by waves generally had a greater influence on sediment transport and deposition than the relatively lamina tidal flow, and planar surfaces were prevalent on the higher

parts of the sand bodies whereas scour megaripples that are generally produced by the tidal currents were occassionaly present as "remnant" scour pits in these planar surfaces. Although the forces of tidal flow and wave surge were both generally onshore, there appeared to be a relationship between wave surge and the amount of grains being transported. The directions of fluorescent grain depletion from the release points tended to correspond to the directions of dominant wave-surge (induced by interfering wave crests) rather than the direction of tidal flow. High concentrations of fluorescent grains and closely spaced isopleths of tagged-grain concentrations correspond to the zones where the predominant force was produced by wave interference rather than tidal flow. A more detailed description of the structures and processes associated with these areas is presented in Oertel (1972).

Intertidal Surfaces and Tidal Current - Longshore Current Interactions

The foreshore zones adjacent to the south end of Sapelo Island also experienced ebbing and flooding tidal streams. The interaction of these tidal currents with wave-induced longshore currents illustrated some patterns of sediment drift that have not been discussed above. In the nearshore zone, wave-surge was not able to pass across the shallower portions of the sea bed into deeper water as it did on the offshore sandbanks (described above), instead the onshore residual surge of waves "piled-up" water in front of the beaches and produced longshore currents. These wave-induced currents were a relatively continuous flow of water, unlike the above described periodic wave-surges that were related to the periods of assymetrical waves. Tidal currents and longshore currents adjacent to the beach were in mutually evasive zones and interactions only took place along the line of breaking waves bordering the two zones (Figure 6a). Wave-induced currents that formed landward of the line of breaking waves were a very turbulent flow of water and consequently a relatively large amount of sand was temporarily transported in suspension (Ingle, 1966). Tidal currents seaward of the line of breakers were less turbulent than the wave-induced currents and very little sand was transported in suspension.

The sample grid selected for sand dispersion analysis encompassed an area that straddled the line of breakers and was influenced by tidal currents (seaward of the line of breakers) and longshore currents (landward of the line of breakers). Whereas wave-surge/tidal-current interactions were very typical of areas at offshore sandbanks, interactions were restricted at the beach because the zones of tidal flow and wave-induced flow were generally separated by the line of breakers.

During the ebbing tide, tidal currents in a zone seaward of the line of breaking waves flowed in a direction opposite to the flow of longshore currents (landward of the line of breaking waves). An evaluation

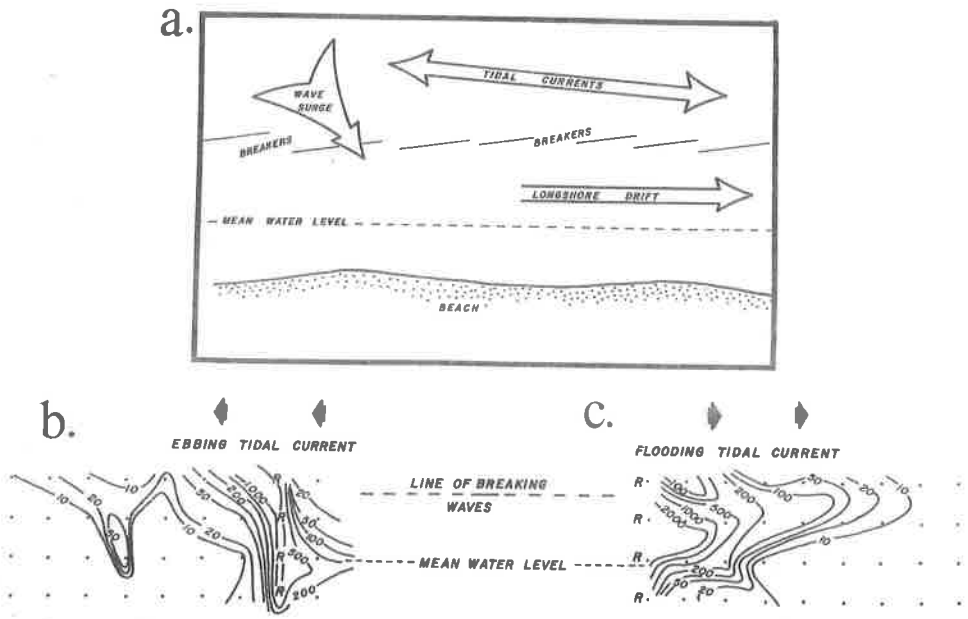

Figure 6(a) Map showing the distribution of nearshore currents at a beach adjacent to an estuary entrance. Longshore currents and tidal currents are in mutually evasive zones separated by the line of breaking waves. (b) Map of isopleth patterns in area depicted in Figure 6a. Ebbing tidal currents seaward of the line of breaking waves flow in the opposite direction of longshore currents landward of the line of breaking waves and sand drift landward of the line of breakers is also opposite to sand drift seaward of the line of breakers. (R) designates release points of fluorescent sand. (c) Map of isopleth patterns in area depicted in Figure 6a. The ebbing tidal current flows parallel to the direction of longshore drift. (R) designates release points of fluorescent tagged sand.

of isopleth patterns in the offshore portion of the grid indicates that the transport direction of tracer grains was northward and corresponded to the direction of tidal flow, while in the landward portion of the grid, grains were transported southward and opposite to the direction of tidal flow (Figure 6b). The flow directions on the landward side of the grid corresponded to the directions of longshore currents and swash currents. Since the sand bed at the beach was generally a planar surface, there were no local concentrations corresponding to the margins of bedforms. However, some anomalously high concentrations were present and may have been produced by rip currents or the occasional surge of very large waves. Since, the crests of breaking waves did not form a continuous line across the center of the sample grid, an exchange of

sediment was possible through this segmented line of breakers (Figure 6). An exchange of sediment of this type is illustrated in Figure 6b by the anomalously high concentration in the middle of the sample grid. This anomalous concentration was apparently the result of a set of large waves which began surging seaward of the "average positon" for the line of breaking waves. The onshore surges of water associated with these large waves apparently produced shoreward transfers of sediment from the zone normally limited to tidal flow, across the line of breaking waves into the zone of longshore drift. In contrast, rip currents may be capable of producing offshore transfers of sediment across this segmented line.

During the flooding tide, longshore currents and tidal currents were both in an alongshore direction toward the adjacent tidal inlet. Tagged grains were transported down current from the release points with maximum grain-transport along and parallel to the line of breakers (Figure 6c). In the swash zone, isopleth patterns illustrated a second direction of sand transport that was parallel to the flow of swash currents (Figure 6c). These patterns of grain transport were very similar to isopleth patterns illustrated by Ingle (1966), however, an offshore direction of sediment transport did not emerge from the data collected here.

CONCLUSIONS

In nearshore areas adjacent to Georgia estuary entrances, wave-current/tidal-current interactions are common, patterns of sand dispersion are very complicated, and the steep sides of bedforms are not always oriented normal to the direction of maximum current velocity or to the direction of longest duration of water flow. The relatively deep subtidal areas around shoal margins generally have relative wave heights (wave height/depth of water under wave crest) less than 0.2 and a time-velocity assymetry of wave surge is not common. In these areas, tidal currents are more important than waves in transporting sand, and sand is predominantly transported in linguoidal and cuspate dunes. The slipface orientations of these dunes, and the directions of the longest distances of sediment transport correspond to the directions of the tidal currents.

At shallow subtidal surfaces (exposed only during low water at the spring tides), the relative wave heights are generally larger than 0.4 and onshore wave-surge appears to be a major factor determining the long axis of bedforms. The greatest distances of sand transport remained in the same direction as the tidal flow even in cases where the onshore surges of waves tended to inhibit tidal flow to the point of severe dune modification. In areas having wave-surge/tidal-current interactions and illustrating dune modifications, bedforms tended to be oriented almost parallel to the direction of wave-surge rather than

normal to the direction of tidal flow. Thus, wave surge appeared to be the major factor aligning these bedforms although tidal currents transported sand the greatest distances, and although the directions of tidal flow generally correspond to the longest distances of grains transport, bedform orientations at shallow subtidal surfaces are not always reliable indicators of tidal-flow directions.

At shallow intertidal portions of a sand shoal, the forces of wave surge occasionally overwhelmed the forces of the flooding tidal currents and as a result, bedforms and patterns of sand dispersion were predominantly controlled by the approach directions of surging waves. Refraction produced two sets of wave-crests moving onshore that crossed each other at acute to obtuse angles. These two sets of refracted and shoaling waves caused surges of water to move toward the long axis of the shoals and sand entrained by these surges was transported from shoal margins toward the shoal axis. A third direction of onshore surge was produced along the points of interference between the two refracted wave-sets, and the force of this third onshore surge of water was generally greater than either of the two component forces. The resultant force created from the interaction of surging waves, produced a turbulent, onshore transport of sand along the central portion of the shoals and ultimately determined the orientation of the shoals (Oertel, 1971).

A turbulent flow of sand and water is produced in gyres when ebbing currents interact with interfering wave-crests. The sedimentary record of these gyres was not readily discernible in the low-angle stratification of the substrate below planar surfaces, however, observations indicate that the low-angle stratification is the record of sand deposition from turbulent, surging and breaking waves. Low-angle stratification is also produced by conditions of the transition and upper flow-regimes; however, these strata were not deposited in an upper-flow regime.

At the shoreline, breaking waves transported water onto the foreshore where it accumulated in a zone between the breakers and the beach. The resultant direction of longshore flow was parallel to the beach and was determined by the approach direction of wave crests. Tidal currents were also parallel and adjacent to the beach but were restricted to a zone just seaward of the line of breakers. When the longshore currents and the tidal flow were in opposite directions, the direction of sand transport on the landward side of the line of breakers was opposite from the direction of sand transport on the seaward side of the line of breakers. An exchange of sand across the line of breakers occasionally occurred whereby sand was transported into the zone of longshore drift by the occasional surges of large waves or sand was transported seaward into the tidal current zone by rip currents.

Bedform configurations in mesotidal nearshore environments may be useful geologic indicators for detecting the presence and the nature of the interactions of wave-surge and tidal currents. The intertidal parts of nearshore shoals generally illustrate large planar surfaces

that are characteristic of turbulent sedimentation processes of surging and breaking waves. The long axis of these large planar bedforms (swash platforms, Oertel, 1971) generally bisects the angle between the two approach directions of refracted wave-crests. At "deeper-water" margins around these bedforms, flat, linear-crested megaripples are oriented by turbulent surges of water and have trends parallel to the two respective wave-approach directions on the opposite sides of an offshore sand shoal. These linear, flat-topped megaripples and flat-topped sand waves on the margins of offshore shoals may be useful geologic indicators for deciphering the nature of refracted waves. At yet "deeper-water" margins around sand shoals, bedforms are no longer oriented by wave approach and linguoidal and cuspate dunes form slip faces on the down tidal-current sides. Dunes migrate in response to the flow of tidal currents and the orientations of these dunes are useful in determining complicated patterns of ebb and flood channel systems.

REFERENCES

Harms, J. C. and Fahnestock, R. K., 1965, Stratification, bedforms and flow phenomena (with an example from the Rio Grande): p. 84-115, in Middleton, G. V. (editor) Primary sedimentary structures and their hydrodynamic interpretation: Society of Economic Paleontologist and Mineralogists, Special Pub. No. 12, Tulsa, Oklahoma.

Hayes, M. O., 1972, Diagnostic sedimentary structures of mesotidal barrier beaches: (Abstract, p. 624 of Program) Ann. Meeting Soc. of Econ. Pal. and Min., Denver, Colorado.

Ingle, J. C., 1966, The movement of beach sand: Developments in Sedimentology 5, Elsevier Publishing Company, Amsterdam, London, New York.

Inman, D. L. and Nasu, N., 1956, Orbital velocity associated with wave action near the breaker zone: Tech. Memo No. 79, Beach Erosion Board, Corps of Engineers.

Jolliffe, I. P., 1963, A study of sand movements on the Lowestoft sandbank using fluorescent tracers: Geographical Journal, v. 129, p. 480-493.

Oertel, G. F., 1968, Structures and processes of a marine-estuarine environment: Unpublished Masters Thesis, University of Iowa, Iowa City, Iowa.

_____, 1969, Structures and processes of a marine-estuarine environment: (Abstract, p. 35 of program) Ann. Mtg. of North Central Geol. Soc. America.

_____, 1971, Bores of interfering waves; an important factor in nearshore shoal development: (Abstract) p. 271 of Abstract Volume, Second National Coastal and Shallow Water Research Conferences, Newark, Delaware.

Oertel, G. F., 1972, Sediment transport on estuary entrance shoals and the formation of swash platforms: Jour. Sed. Pet., v. 42, p. 857-863.

Oertel, G. F. and Howard, J. D., 1972, Water circulation and sedimentation at estuary entrances of the Georgia coast, in, Shelf sediment transport: Process and pattern, (D. J. P. Swift, D. B. Duane and O. H. Pilkey, eds.) Dowden, Hutchinson and Ross, Stroudsburg, Penn.

Robinson, A. H. W., 1966, Residual currents in relation to shoreline evolution of the east Anglian coast: Mar. Geol., v. 4, p. 57-84.

Simons, D. B., Richardson, E. V. and Nordin, C. J. Jr., 1965, Sedimentary structures generated by flow in alluvial channels, in Middleton, G. V. (ed.) Primary sedimentary structures and their hydrodynamic interpretation: Society of Econ. Paleontologists and Mineralogists, Special Pub. No. 12, Tulsa, Oklahoma.

Swift, D. J. P., 1969, Lecture 4: Inner-shelf sedimentation: processes and products, in Stanely, D. J. (ed,)The new concept of continental margin sedimentation: Amer. Geol. Inst. 2201 M. Street, N. W., Washington, D. C. 20037.

Tanner, W. F., 1960, Expanding shoals in areas of wave refraction: Science, v. 132, p. 1012-1013.

A SEISMIC ESTIMATE OF DEPTH OF TRIASSIC DURHAM BASIN, NORTH CAROLINA

By

David M. Stewart
J. A. Ballard(1)
and
William W. Black

Geology Department
University of North Carolina
Chapel Hill, North Carolina

ABSTRACT

A seismic measurement of depth to basement has been made near the center of the Triassic Durham Basin between Chapel Hill and Raleigh, North Carolina, and indicates that the probable depth of sediments there is 6,000 ± 500 feet. No velocity data is available for the Triassic rocks of the Durham Basin and therefore, depths and dips calculated from the seismic data must be considered preliminary. This estimate is based on velocity measurements made on Newark Triassic rocks in South Carolina by refraction seismology (Wollard, et al, 1957) and on two sonic logs from wells in the buried Triassic Dunbarton Basin in South Carolina. Quantitatively, the reflection data indicates that the beds dip toward the east and increase gradually from 20° at the surface to probably no more than 30° near the bottom. The basin bottom has no dip and seems to be overlain by another layer 50-100 feet thick also with no dip. There are numerous reflection horizons that may be no more than indications of the typical Triassic sequences of alternating sandstones, siltstones, and shales. However, three unusually strong reflectors, dipping concordantly and followed by apparent multiples, suggest sills 50-200 feet thick. One good reflector with an angle of emergence toward the west suggests a dike and/or fault dipping at 70°-90°W. A brief magnetic survey at the projected outcrop indicated nothing that could be interpreted as a dike. A curious (N-S, E-W) latent joint pattern observed around the shot holes might be related to the present and/or past state of stress for these rocks and for the whole basin.

(1) Present Address: U. S. Naval Oceanographic Office, Chesapeake Beach, Maryland 20732.

INTRODUCTION

The Triassic Deep River Basin is about 90 miles long extending from about 25 miles south of Sanford, N. C., to about 25 miles north of Durham, N. C. The northern half is referred to as Durham Basin while the southern half is called Sanford Basin. The Triangle Brick Quarry is located almost exactly in the center of Durham Basin which is about 10 miles directly south of Durham.

At the Triangle Brick quarry, soft partially weathered claystone and siltstones are 20 to 25 feet thick with interbedded arkosic sandstone about 2 to 3 feet thick. In outcrop, the average dip is 20° to the east. No dikes or other intrusives are visible in the quarry. The excavation of these materials--all of which are used in the production of brick--has produced a bedrock quarry floor 25-75 feet below the natural surface.

Triassic sediments in the Deep River basin are divided into 3 units. The lower unit (Pekin) outcrops along the northwestern boundary and is a conglomerate interbedded with arkosic sandstones, siltstones and claystones. The upper unit (Sanford) outcrops along the southeastern side of the basin and is composed of a coarse fanglomerate in the immediate vicinity of the Jonesboro fault and also interfingers with inner sediments similar to those of the Pekin formation. The middle unit (Cumnock) is coal bearing in the Sanford portion of the Deep River basin, but may not be present in the Durham basin (Reinenund, 1955). These units may be thought of as lateral facies rather than a true vertical sequence.

Triassic or younger dikes cut the entire stratigraphic column, and are also present outside the basin. They are usually emplaced in pre-existing planes of weakness such as faulted zones. One possible sill 3 1/2 miles to the north at the intersection of N. C. 55 and 54 was noted by Singh (1963), otherwise they are rare in the Deep River basin. There are no definitely documented lava flows south of Virginia in the Triassic basins.

Large fault block, or horsts, have been suggested as being present in the floor of the basin and are now covered by sedimentary rocks. Such a block may exist in the vicinity of the Wadesboro basin (Randazzo, et al., 1970). Gravity profiles in the Deep River basin also suggest horsts in the basement (Mann and Zablocki, 1961). I. W. Marine (Personal Communication, 1972) also has explained gravity anomalies in the buried Dunbarton basin in this way.

Previous estimates of thickness of sediments overlying the pre-Triassic basement in the Durham Basin range from 3,100 feet (Mann and Zablocki, 1961) to more than 10,000 feet (Prouty, 1931). A trigonometric projection of the observed 20° dip six miles eastward to the Jonesboro fault indicates a thickness of nearly 12,000 feet. If, as seems likely from the stratigraphy, initial dips were increased by post-depositional movement along the boundary fault, then initial dips can be

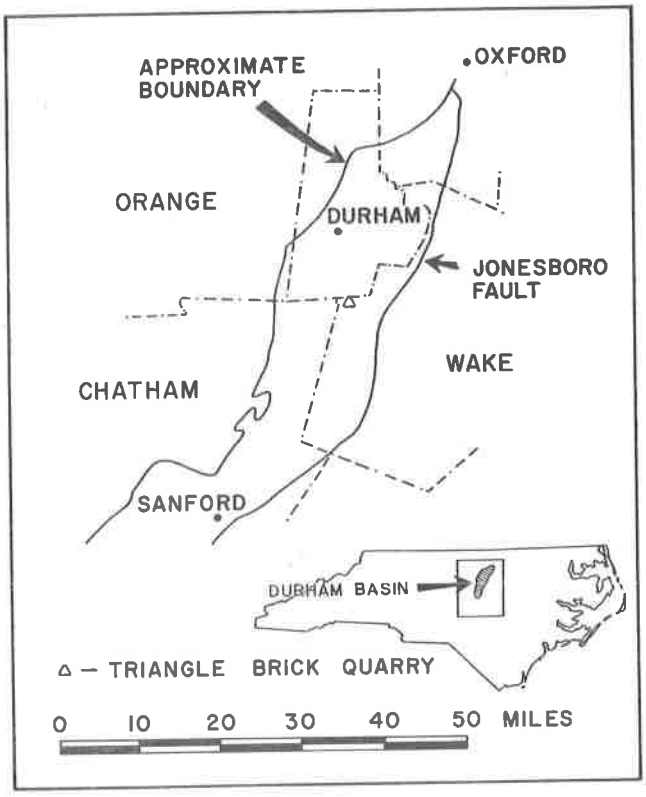

Figure 1. Location map for Durham Basin.

estimated as 10°-12° thus making it unlikely that the basin depth at the site of the seismic measurements exceeds 6,000-7,000 feet.

Acknowledgments

We sincerely express our appreciation to the Triangle Brick Company, and especially to Ted Tysinger who represented them, for their full cooperation. They not only offered their quarry as a site for the seismic measurements, but actively participated in the project by grading the quarry floor to simplify the laying of geophone lines and by drilling the shot holes. We wish to thank I. W. Marine of the DuPont Company and N. Stetson of the Atomic Energy Commission for allowing us the use of two sonic logs taken in the Dunbarton Basin. Appreciation goes to George L. Bain of the U. S. Geological Survey for his help and encouragement. Thanks also goes to U. N. C. students Joseph Wooden and Bruce Hurley who did the surveying and to Gertrude Gunia, George

Birchard, Neil Murphy, Thomas Ellsworth, and Thomas Hawkins, all of whom assisted in the field work.

FIELD PROCEDURES

The equipment used was an Electrotech Portable Refraction Seismic System with eight geophones. Shot lines were laid along strike (N-S) and across dip (E-W) in a "T" pattern. The spread along strike was 550 feet, and that across dip was 650 feet. The shot holes were all water filled and six feet deep in hard sandstone. Dynamite charges varied from 1/2 to 4 pounds. A total of seventeen records were made on two different occasions using a variety of amplifications and filters to optimize records. The area was seismically very quiet so that little or no filtering was needed. The agreement between shot records for individual reflection is good to excellent. Many weaker reflections were undoubtedly obscured because of instrument limitations. The data listed in Table 1 is a synthesis of all seventeen records.

VELOCITY DATA FOR NEWARK TRIASSIC ROCKS

Seismic reflection data consists of two way travel times and cannot be translated into depths and dips unless seismic velocities in the rocks and the manner in which velocity varies with depth are known. Refraction data normally provides direct velocity measurements, but our's did not penetrate below 100 feet. No other seismic velocity data exists for the Durham basin. It is possible to generalize from similar rocks in other areas. Several sources exist. Faust (1951) gives data on Triassic sandstones and shales for Montana, North Dakota, Wyoming, Colorado, New Mexico and Louisiana. These velocities range from 7,500 fps at 700-1,500 feet depth to 12,500 fps at depths in excess of 7,000 feet. Below 1,000 feet, velocity increases proportionally to the 6th root of the depth. The velocities of Faust are typical of sandstones, siltstones, and shales in most places (Grant and West, 1965). The refraction studies of Wollard, et al., (1957), over buried Triassic rocks in South Carolina indicate these rocks have average velocities of at least 11,000 fps below 500 feet depths and exceed 19,000 fps below 3,000 feet. Two recent sonic logs were obtained with the cooperation of I. W. Marine and N. Stetson from the Atomic Energy Commission and the DuPont Company, Savannah River Laboratory, Aiken, South Carolina. These logs were made in test holes in the buried Triassic Dunbarton Basin in South Carolina. One was near the edge of the basin and beneath the Coastal Plain sediments penetrated Triassic fanglomerates over 2,000 feet thick and into an augen gneiss basement below. An average velocity for the Triassic portion of this log was nearly 15,000 fps and in this case did not change appreciably with increased

Table 1. Seismic Reflection Data with Remarks.

Event Number	2-Way Reflection Time (Seconds)	Emergence Angle	Remarks
1	.18*	19° E*	
2	.25	18° E	
3	.31	17° E	Possible sill top
4	.33	17° E	Possible sill bottom
5	.35	16° E	Possible multiple
6	.39	16° E	Possible sill top
7	.41	15° E	Possible sill bottom
8	.43	15° E	Possible multiple
9	.45	14° E	Possible multiple
10	.49	14° E	
11	.51	13° E	Possible sill top
12	.52	13° E	Possible sill bottom
13	.53	12° E	Possible multiple
14	.56	12° E	
15	.60	11° E	
16	.63	11° E	
17	.67	11° E	
18	.69	10° E	
19	.73	10° E	
20	.77	10° E	
21	.79	33° W	
22	.82**	0°	Top of weathered basement (?)
23	.83**	0°	Floor of Basin (?)

*These values are averages obtained from consideration of seventeen records. Two-way reflection times were determined to the nearest .01 seconds and may be considered accurate to $\pm$ .005 sec. Emergence angles were determined to $\pm$ 3° in the vertical and $\pm$ 10° in the horizontal. Hence, 19°E may be read 19° $\pm$ 3°, E $\pm$ 10°. Greater accuracy was not possible due to limitations of the equipment. The absence of reflection data before .18 sec. is due to noise levels in the early parts of the records rather than geology. Events were there but accurate times were unobtainable. .18 sec. corresponds to the top 700-900 feet. Refraction data is available for the top 60 feet (see Figs. 2, 3 and 4).
**The .82 and .83 events werevery strong. No reflection events were recorded after these even though the records extended well beyond one second.

depth. The second log was near the center of the basin (very near Wollard, et al. station #59) and penetrated over 3,000 feet of Triassic

rock beneath the Coastal Plain sediments. The Triassic rock velocities increased steadily from about 15,000 fps at 1,000 feet depth to over 19,000 fps below 4,000 feet. It is reasonable to assume that the velocities obtained by Wollard, et al., (1957), the sonic logs from Dunbarton Basin, as well as the surface measurements we made at Triangle Brick are probably much closer to the true Durham Basin velocities than those of Faust (1951). The fact that available East Coast Triassic rock velocities are considerably higher than the more typcial values of Faust (1951) may be due to present day stresses and/or past tectonic forces affecting these sediments.

REFRACTION DATA

Because the spread lengths were short, and because dipping beds lessen the depth of penetration of refracted arrivals, no refraction data was obtained below 100 feet. Figure 2 is a plot of the forward and reversed first-break profiles shot along strike. The near perfect symmetry of the forward and reversed refraction profiles and the fact that all reflected emergence angles were zero confirms that this spread was very close to true strike.

The geophone line was on a loosely consolidated clay rich fill and was parallel to a small stream channel whose bed was hard sandstone. The velocity of the fill in which the geophones were placed is 5,000-6,100 fps. This fill is no more than 10-14 feet thick anywhere along the spread. The geophones 250 to 400 feet from the shot point (Figure 2) show an apparent negative velocity. This is evidence of a low velocity layer below the outcropping sandstone. Because this low velocity material underlies a high velocity material, it is impossible to calculate the thickness of the sandstone outcropping in the stream. However, it is possible to obtain a good approximation of the thickness of the sandstone plus the low velocity bed and thus obtain the vertical distance to the top of the bed below. This bed is about 60 feet below the surface (Figure 3).

Figure 4 is a plot of the forward and reversed first break profiles taken across true dip. As can be seen, they are very irregular with different apparent velocities between virtually every geophone. The apparent velocities between phones range from a low value of 4,000 fps to a high of 500,000 fps (nearly infinite), and include a negative velocity of -20,000 fps. This velocity distribution pattern is a result of the 20° dip and alternation of low and high velocity beds. Maximum vertical penetration for these dip refraction profiles is less than 100 feet. Thus, both spreads of refraction only give information about the near surface and corroborate what can be deduced from the exposures seen in the sides of the pit.

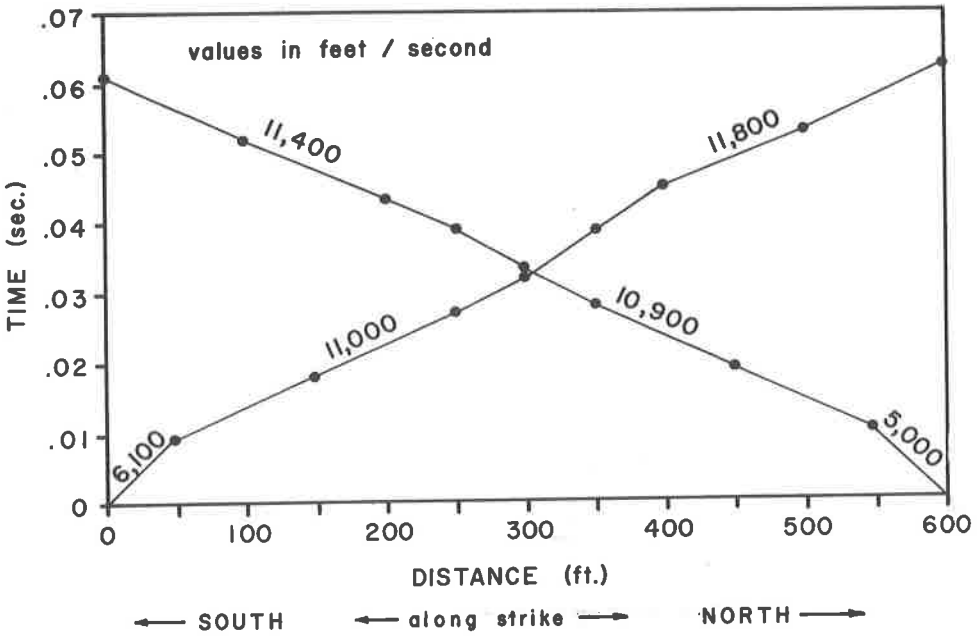

Figure 2. Forward and reversed refraction profiles along strike.

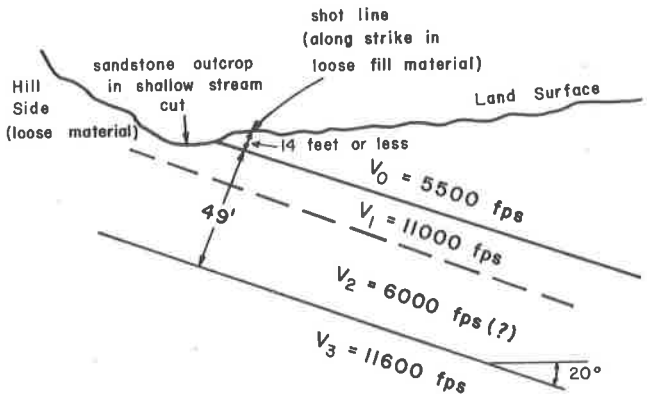

Figure 3. A geologic interpretation consistent with refraction data.

REFLECTION DATA

The reflection data obtained by this survey are presented in Table 1. The figures given there are averages obtained from seventeen records taken from two profiles along strike and two profiles across dip at the Triangle Brick Quarry. If velocity is constant with depth,

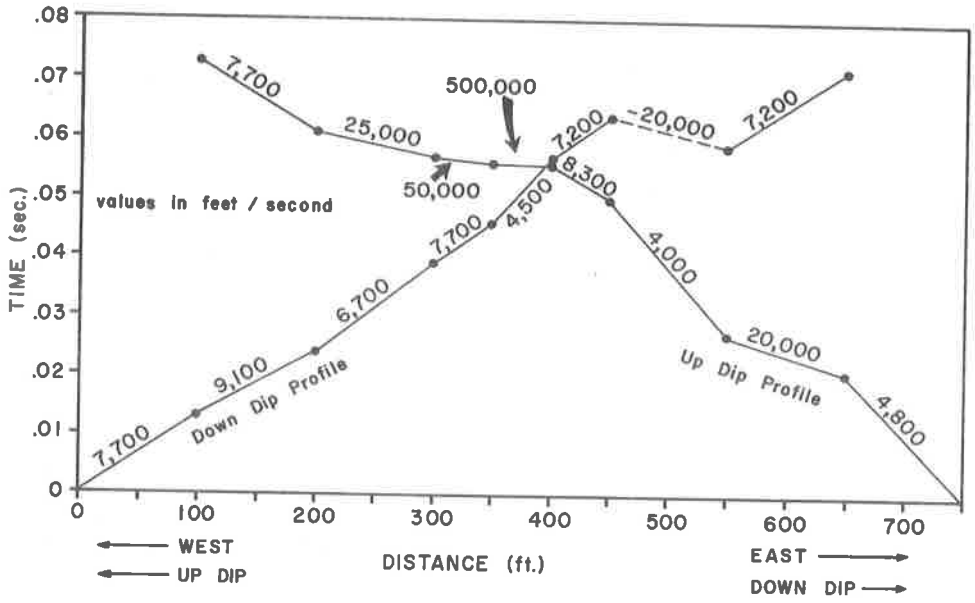

Figure 4. Forward and reversed refraction profiles across dip.

then seismic ray paths are straight and emergence angles correspond to true angles of dip. However, velocity almost invariably increases with depth which means that ray paths are curved and true dip angles are generally greater than emergence angles. Assuming that velocity does increase with depth, the gradual decrease in emergence angles from 19° to 10° for deeper and deeper reflections probably corresponds to a gradual increase in dip with depth. The actual magnitude of this increase cannot be determined without knowing the manner in which velocity does increase with depth, but based on the data of Faust (1951) the true dip of the lowest eastward dipping bed (event 20) cannot be less than 20°-22° and based on the higher velocity of other Newark Triassic rock could be as much as 35° which should be considered a high limit. These dip estimates are calculated from emergence angles assuming a linear velocity variation with depth and employing formulas given and discussed on pages 145-149 of Dix (1952).

The reflection data appears to extend to the very bottom of the basin. The last event (at 0.83 seconds) is strong and has a zero angle of emergence for both the spreads-along strike and across dip. Hence, true dip is zero. Furthermore, no events are recorded after 0.83 seconds. This strongly implies that the 0.83 second event is from the bottom of the basin.

The actual depth corresponding to this two-way time will not be known until good velocity data is available for Durham Basin, but estimates can be made from data obtained elsewhere. Based on Faust's (1951) data, the minimum depth is 3,700 feet, the maximum 4,500 feet. Depths based on other Newark Triassic rock velocities range from 5,500

to 6,700 feet. It seems likely that the Durham Basin at the Triangle Brick Site is at least 5,000 feet deep and is probably nearer 6,000. A value of 6,000 ± 500 feet would be a good estimate. The lack of precise velocity data limits the usefulness of our estimate, but is, nevertheless, more quantitative than any previous estimate.

A consistent characteristic of the 0.83 second event is that it is a multiple event: the 0.82 and 0.83 reflections are clearly distinct events. The 0.82 event also has zero dip. This may represent a weathered zone in the basement or a horizontal sedimentary layer on top of the basement. The thickness of this layer is probably not less than 50 feet nor more than 100 feet.

Event 21 at 0.79 seconds has an emergence angle at 33° ± 3° to the west. All earlier events emerge toward the east at angles less than 20°. This reflector is defined for several hundred feet in all directions, and is displaced toward the east. Faust's data indicates that the true dip of this reflector cannot be less than 45°, but based on more realistic velocity data, the dip is more likely to be 70-90°. This suggests the presence of a dike, a fault, or a dike in a fault plane. If it is a dike, projected outcrop would be 0.5 to 0.9 miles east of the Triangle Brick Site. A magnetic traverse revealed no anomaly that could be interpreted as a dike. A number of workers have suggested the presence of horsts in the floor of the basement. This plane could be one side of a completely buried horst.

Events 3, 6, and 11 at 0.31, 0.39, and 0.51 seconds respectively are strong and followed by what may be multiples. Since there dips are conformable to the sediment, these reflectors may be sills or unusually thick, well consolidated, sandstones which are characteristic of the Newark Triassic basins. Only a test hole at this site could determine the nature of these strong reflectors. Their thicknesses would be 100-200 feet for the top two and 50-100 feet for the bottom one. No sandstone beds of such thickness are known at the basin's surface. Depending on assumption of velocity, depths of their tops below the Triangle Brick Company site would be 1,300-2,000 feet, 1,800-2,600 feet, and 2,500-3,800 feet.

THE PRESENCE OF A LATENT JOINT SYSTEM

A curious latent joint system was observed about the shot holes. In a homogeneous, isotropic material a charge detonated in a shallow hole will result in a radial pattern of cracks. At the Triangle Brick Quarry fractures formed around the shot hole after each dynamite blast, but were always in a retangular pattern with one set of fractures oriented N-S and the other E-W. This is roughly parallel and perpendicular to the axis of the basin and to the strike of the dipping Triassic rocks. This must surely be related to the present and/or past state of stress for these rocks and for the whole basin. If, for example, the basin is

presently under compression, this could explain the anomously high seismic velocities of these rocks. There would also be anisotropy with the result that seismic waves would travel at different velocities in different directions--perhaps different velocities N-S than E-W or vertically.

CONCLUSIONS

The figures for the depth of Triassic rocks in the Durham Basin as presented here can only be considered as estimates for several reasons. The velocity input to the calculated depths and dips was all assumed based on velocities of Newark Triassic rocks outside of the Durham Basin. Many small reflection events were obscured by the relatively undamped refraction unit. Even so, the accuracy of the recorded times and angles certainly was better than the extrapolated velocities.

The reflection data indicate that the materials overlying the crystalline basement in the Durham Basin all dip to the East, probably gradually increasing in dip from $20^{o} \pm 3^{o}$ at the surface to no more than 30^{o} at basement, the only exceptions being high-angle faults and dikes. Most of this material is probably Triassic sedimentary rocks, but there may be several sills. The basin floor appears to be horizontal and overlain by another horizontal layer that may be a "weathered zone." Basin depth is at least 3,700 feet by the most conservative velocity estimates and is more likely to be in excess of 5,000, but probably less than 6,700 feet, by the most realistic velocity estimates.

REFERENCES CITED

Dix, C. H., 1952, Seismic prospecting for oil: Harper & Brothers, N. Y.

Faust, L. Y., 1951, Seismic velocity as a function of depth and geologic time: Geophysics, v. 16, p. 192-206.

Grant, F. S. and West, W. F., 1965, Interpretation theory in applied geophysics: McGraw-Hill, N. Y.

Mann, V. I. and Zablocki, F. S., 1961, Gravity features of the Deep River Wadesboro Triassic Basin of North Carolina: Southeastern Geol., v. 2, p. 191-216.

Prouty, W. F., 1931, Triassic deposits of the Durham Basin and their relation to other Triassic areas of Eastern U. S.: American Jour. Sci., v. 21, p. 473.

Randazzo, A. F., Swe, W., Wheeler, W. H., 1970, A study of tectonic influence on Triassic sedimentation--The Wadesboro Basin, central Piedmont: Jour. Sedimentary Petrology, v. 40, p. 998.

Reinemund, J. A., 1955, Geology of the Deep River Coal Field, North Carolina: U. S. Geol. Survey Prof. Paper 246.

Singh, H., 1963, Diabase intrusion of a portion of the Durham Triassic Basin, North Carolina: unpublished M. S. Thesis, University of N. C., Chapel Hill.

Wollard, G. P., Bonini, W. E., and Meyer, R. P., 1957, A seismic refraction study of the subsurface geology of the Atlantic Coastal Plain and continental shelf between Virginia and Florida: Wisconsin U. Dept. Geology Tech. Rept., Contract N70NR-28512.

PARAGENESIS OF AN UNUSUAL HYDROTHERMAL ZEOLITE ASSEMBLAGE IN A DIORITE -- GRANITE CONTACT ZONE WOODLEAF, ROWAN COUNTY, NORTH CAROLINA

By

Donald R. Privett
Department of Geology
Catawba College
Salisbury, North Carolina 28144

ABSTRACT

The contact between an intrusive granite to quartz monzonite stock and host diorite has been exposed in a large crushed stone quarry located at Woodleaf, eight miles northwest of Salisbury, North Carolina.

Hydrothermal solutions permeated and metasomatized both the granite-quartz monzonite and diorite producing widespread replacement and fracture filling prehnite; followed by the calcium zeolites: laumonite, scolecite, chabazite, heulandite, and stilbite.

The prehnite and laumontite are most abundant. Prehnite occurs as : (1) massive light green fracture filling and replacement veinlets (2-6 cm wide) in diorite that commonly contains vugs filled with small subhedral crystal groups. (2) a pale green fine-grained metasomatic replacement of the granite-quartz monzonite.

Laumontite, the most common zeolite, is present as: (1) vug and fracture filling euhedral, enamel white crystals and intergrown prismatic crystal groups. (2) interlacing fracture filling veinlets of pink acicular crystals in the granite; (3) pseudomorphs after plagioclase in metasomatized diorite and quartz monzonite.

The other zeolites (chabazite, heulandite, stilbite, and rare scolecite) occur as euhedral crystals and crystal groups on fractures and in druses in the granite and diorite. Plagioclase (An_{27}), chlorite, calcite, quartz, pyrite and chalcopyrite occur in thin joint planes and in small vugs in both the granite and diorite. Rare fluorite fills interstices in granite breccias and occurs with epidote replacing granite along fractures. Molybdenite occurs on joints in the granite, in drusy quartz veins of the diorite, and in small microcline veinlets.

INTRODUCTION

An excellent contact reaction zone between an intrusive granite to quartz monzonite stock and host diorite has been exposed in a large crushed stone quarry (0.5 mile long, 0.3 mile wide and at least 165 feet

Table 1. Optical Data for the Zeolites and Associated Minerals.

Mineral	Index of refraction	Optic sign and 2V	Optical orientation	Extinction angle
white laumontite crystals	α = 1.510 γ = 1.524	Biaxial (-) 2V=40-45°	length slow	inclined 9-10°
pink asicular laumontite-leonardite	α = 1.508	Biaxial (-)	length fast and slow	inclined 42-40°
chabazite	ω = 1.488	Unaxial (-)		
stilbite	α = 1.486 γ = 1.504	Biaxial (-) 2V=40°	length fast	parallel and undulose
heulandite	β = 1.505	Biaxial (+) 2V=60°		
scolocite	α = 1.508	Biaxial (-)	length slow	inclined
prehnite	α = 1.616 β = 1.622 γ = 1.642	Biaxial (+) 2V=40°		parallel
chlorite	γ = 1.580	Biaxial (-) 2V=30°		parallel

deep) located in the Central Piedmont at Woodleaf, North Carolina eight miles northwest of Salisbury, Rowan County, North Carolina.

Calcium-rich hydrothermal solutions from a granite-quartz monzonite stock produced widespread metasomatic and fracture filling minerals in both the intrusive and diorite host. This study provides optical and x-ray data and discusses the paragenesis of the zeolites and other hydrothermal minerals found in the contact zone.

Most minerals were first identified optically from crushed mineral fragments using Cargille index oils. Optical data is tabulated in Table 1. Optical identifications were later confirmed by x-ray diffraction. X-ray diffraction data were obtained using Ni filtered Cu radiation, tube at 35 kv, 15 ma, 1° divergence silt, 0.01 inch receiving slit. Most samples were run from 60-8° 2θ at 1° 2θ per minute, d values were determined using (λ = 1.542 Å) with mid-point measurement for d at two-thirds the peak heights. Thin sections were studied in order to identify minerals, determine replacement reactions, and to estimate modes.

GEOLOGIC SETTING AND GEOLOGY AT WOODLEAF QUARRY

The rocks exposed in the quarry represent the Charlotte belt; which is one of four geological divisions of the Piedmont of Central North Carolina (King, 1955). From west to east these are the Inner Piedmont, Kings Mountain belt, Charlotte belt and Carolina slate belt. The Charlotte belt is composed of medium to high-rank metamorphics intruded by a wide variety of plutons. In Rowan County the Charlotte belt is represented by mixed diorite and granite intruded by a complex sequence of granites, quartz monzonites, gabbro, altered ultramafics and diabase dikes.

Woodleaf Quarry exposes the contact between a younger unmetamorphosed granite to quartz monzonite stock and a host diorite. The fluid and intrusive nature of the granite is shown by abundant dikes and sills, diorite xenoliths and roof pendants (Figure 1, A and B). Flow around the larger diorite xenoliths is very common. Granite dikes cut the xenoliths (Figure 1, C) and flow aligned biotite schlieren are common (Figure 1, D). Unusual veinlets (3-6 cm) of white microcline containing disseminated molybdenite crystals cut the granite. Both the granite and diorite are cut by late stage vuggy quartz veins containing abundant euhedral crystals of pyrite, quartz, epidote, chalcopyrite, molybdenite, calcite and zeolites.

The host diorite, the xenoliths, roof pendants and intrusive granite are metasomatized. Diorites near the contact with the granite, and diorite xenoliths are commonly laumontized; the granite has been prehnitized and laumontized. Calcium rich hydrothermal solutions moving along joints in the granite crystallized laumontite, $Ca(AlSi_2O_6)_2 \cdot 4H_2O$, heulandite, $(Ca, Na_2)(Al_2Si_7O_{18}) \cdot 6H_2O$, chabazite, $(Ca)(Al_2Si_4O_{12}) \cdot 6H_2O$, stilbite, $(Ca, Na_2 \cdot K_2)(Al_2Si_7O_{18}) \cdot 7H_2O$, scolecite, $Ca(Al_2Si_3O_{10}) \cdot 3H_2O$, and calcite. Vugs in the diorite are partly filled with plagioclase, chlorite, laumonite, prehnite, $Ca_2Al_2Si_3O_{10}(OH)_2$ and chabazite crystals.

The Woodleaf granite is medium-grained (0.5-3.0 mm) hypidiomorphic granular, containing microcline, (1.0-3 mm), quartz (3 mm) muscovite and plagioclase (1-4 mm), plus accessory biotite (0.7-1.4 mm), sphene, and secondary epidote (1.5-1.0 mm), chlorite, and calcite. The microcline is always partly and in some cases completely sericitized; plagioclase is commonly epidotized.

The diorite and quartz diorite is medium-grained hypidiomorphic granular containing plagioclase (0.14-2.0 mm) and hornblende (1.5-3.0 mm). Hornblende aggregates (3-4 mm) commonly enclose smaller plagioclase laths, but not to the extent of producing a poikilitic texture. The quartz (1.5-2 mm) is usually an accessory however, some samples contain over 10 percent quartz and are quartz diorites. Accessory biotie (0.5-1.0 mm), and apatite along with secondary epidote (1.0-1.4 mm) and chlorite are present. The plagioclase is commonly saussurtized.

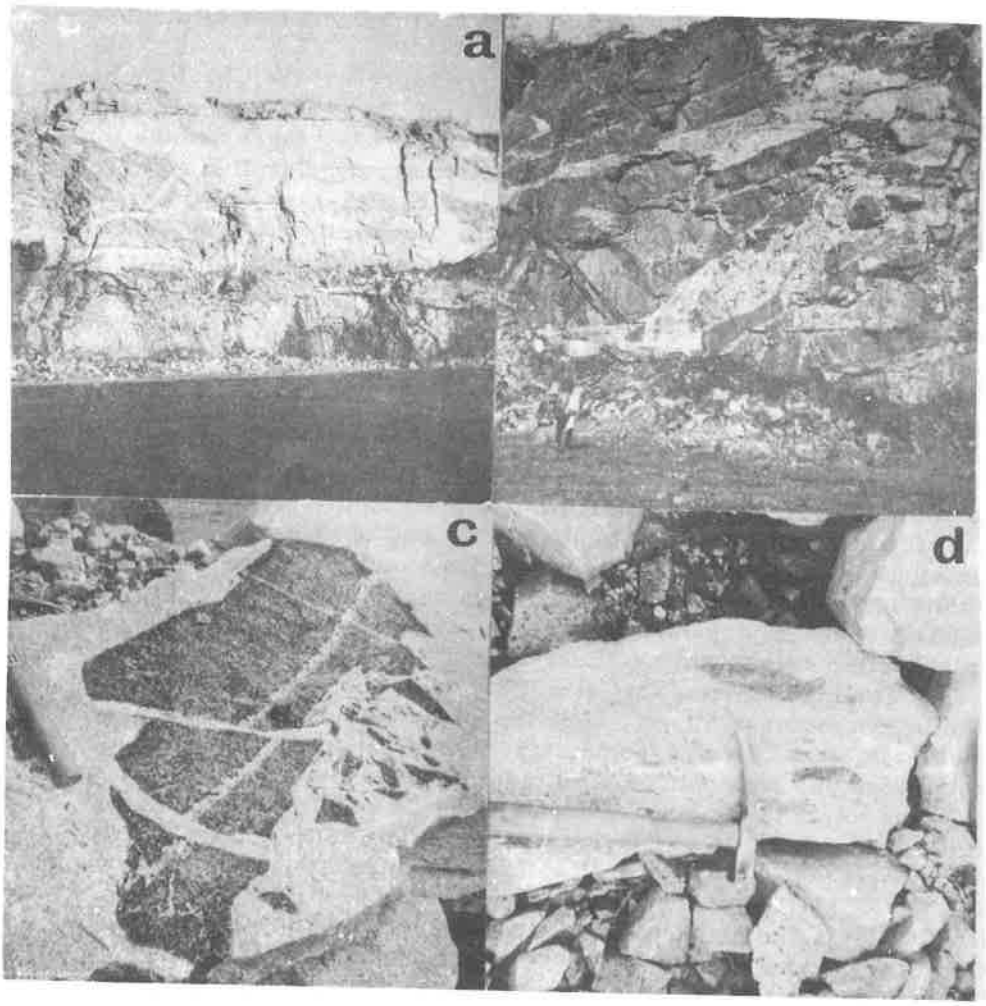

Figure 1. Structures in the rocks at Woodleaf Quarry.
A. Granite dikes and sills (light) intrusive into diorite along the contact zone
B. Granite dikes containing stoped diorite xenoliths
C. A large diorite xenolith cut by succession of granite dikes
D. Flow aligned biotite rich schlieren in granite

DESCRIPTIVE MINERALOGY

Laumontite and prehnite are the most common secondary minerals. Laumontite occurs as : (1) pseudomorphs of laumontite after plagioclase in highly altered diorite and quartz monzonite especially adjacent to prehnite veinlets (Figure 2 A); (2) single euhedral crystals, crystal groups growing from fractures in diorite, and intergrown white

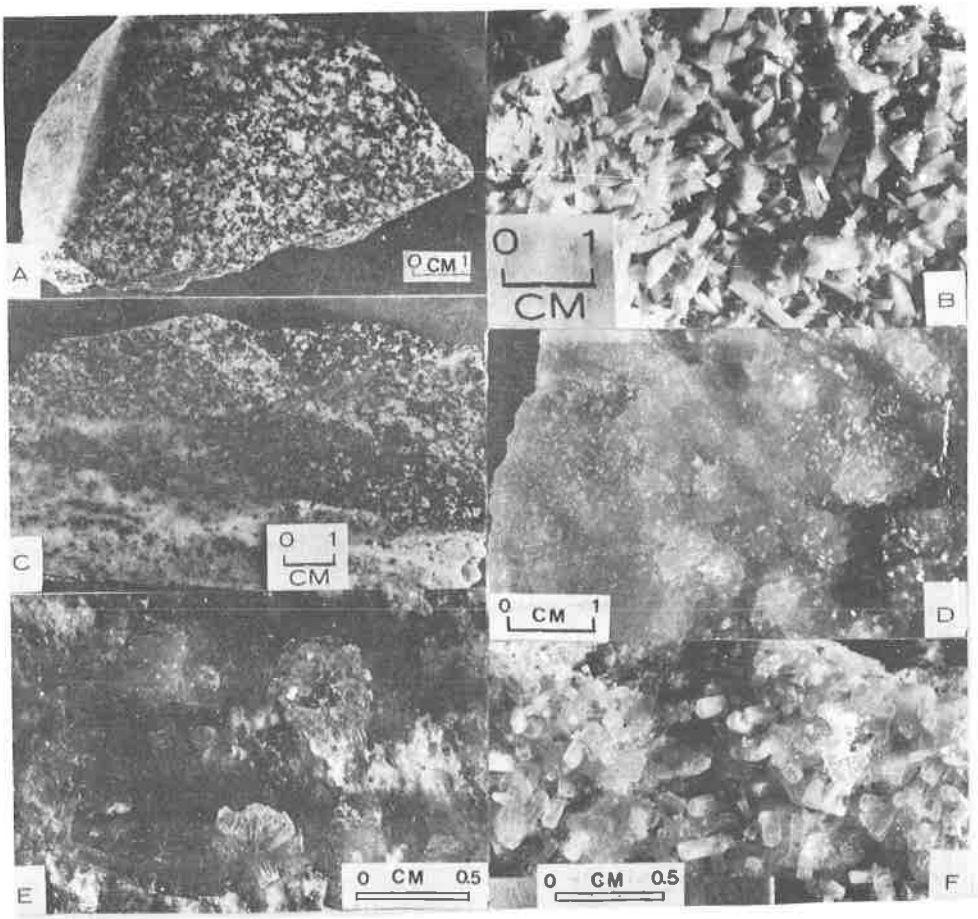

Figure 2. The replacement and fracture filling minerals at Woodleaf Quarry.

A. Laumontized granite adjacent to a prehnite veinlet.
B. Prismatic laumontite crystals on a fracture in granite.
C. Replacement prehnite in diorite.
D. Prehnite crystal clusters.
E. Stilbite and chabazite on fracture in granite.
F. Single stilbite crystals.

subhedral prismatic crystals (Figure 2 B) forming veinlets (up to 1 cm) in the diorite; (3) veinlets of matted acicular pink laumontite filling fractures in altered quartz monzonite.

Euhedral white columnar prismatic crystals of laumontite up to 1.5 cm long by 0.5 cm wide project from open joints in diorite; in some fractures the laumontite nearly fills fractures (up to 1 cm) producing an intergrowth of subhedral prismatic crystals. Single crystals are

also found growing on prehnite and epidote in small druses in the diorite. In some vugs the laumontite crystallized on yellow translucent calcite crystals. The extinction angle is usually higher near the margins, thus indicating the presence of some leonardite.

Laumontite psuedomorphs, after plagioclase, are widespread in altered diorites and granites. The degree of laumontization is most intense (1-2 cm) away from prehnite veins (Figure 2 A) adjacent to joints in the granite and diorites, and in the periphery of xenoliths.

Tiny veinlets (1-2 mm) composed of pink acicular matted crystal aggregates of laumontite-leonardite fill fractures in the altered granite in an interlacing network about 0.7 cm apart. The plagioclase adjacent to the veinlets is always partially replaced by laumonite. The laumontite-leonardite comprises about 20 percent of the rock.

In the less altered diorites, laumontite can be detected only in thin sections. When replacement of the plagioclase is complete, the feldspar develops a pink color, an aid to megascopic identification. Laumontization begins at the anorthite rich centers of zoned plagioclase; in partly altered crystals the more sodium rich outer portions are unaffected.

Both the white cavity filling crystals and the pink acicular laumontite were x-rayed. Laumontite dehydrates to leonardite, the reverse reaction occurs when sample is placed in water, (Coombs, 1952). Also the hydration state varies with the humidity. When examined soon after collection or treated with water, the euhedral crystals are laumontite (Table 2); however, after long exposure to the atmosphere they dehydrate to leonardite. The pink acicular material is mostly leonardite. It should be noted that the data for leonardite (Madsen and Murata, 1970) and for laumontite (Liou, 1971) are very similar. Based upon the spacing of reflections near 1.63 Å (Coombs, 1952) the single crystals analysed soon after collection are laumontite while the pink acicular crystals and single crystals that have been in the laboratory for considerable time (over 6 months) are leonardite.

Prehnite is present as: (1) fracture filling and replacement veinlets in the diorite and granite (Figure 2 C) and (2) as a fine grained metasomatic alteration product of the granite. The prehnite veinlets frequently contain druses in which terminated pale green tabular crystal groups (1-2 mm long and 0.5 mm wide) extend beyond more massive prehnite (Figure 2 D). Calcite and quartz crystals are frequently crystallized on the prehnite.

In the highly altered diorites prehnitization begins with attack of the center of zoned plagioclase crystals as the veinlet is approached prehnitization increases to the point where the original texture is destroyed.

Metasomatism of the granite produced an unusual vuggy pale green rock containing about 20 percent voids (3-5mm). The void surfaces are covered with a coating of tiny prehnite crystals. The only indication of the former existence of a granite is preservation of islands

Table 2. X-ray Diffraction Powder Data Laumontite-Leonardite.

	I		II		III		IV	
hkl(a)	dÅ	I	dÅ	I	dÅ	I	dÅ	I
110	9.52	84	9.50	100	9.44	100	9.43	78
200	6.98	80	6.84	90	6.83	75	6.83	56
$\bar{2}01$	6.23	W	6.19	10	6.18	10	6.18	W
111	5.05	18	5.04	10	5.04	20	5.04	18
220	4.74	30	4.73	30	4.72	14	4.72	16
$\bar{2}21$	4.52	25	4.49	27	4.49	22	4.49	32
130	4.17	100	4.16	95	4.15	100	4.15	100
$\bar{1}31$	3.77	W	3.78	W	3.77	18	3.76	W
$\bar{4}01$	3.67	28	3.66	40	3.65	56	3.66	42
002	3.52	56	3.51	55	3.50	60	3.51	94
131	3.41	16	3.41	10	3.41	16	3.40	26
$\bar{3}12$	3.37	W	3.35	W	3.36	40	3.36	34
040	3.27	50	3.28	50	3.27	60	3.27	63
$\bar{3}11$	3.20	18	3.21	38	3.19	60	3.20	45
330	3.16	32	3.17	20	3.15	32		
$\bar{4}02$			3.07	15			3.09	W
420	3.04	46	3.03	40	3.03	40	3.03	45
240	2.97	W			2.95	W	2.95	W
$\bar{5}11$	2.88	24	2.89	30	2.87	25	2.88	38
$\bar{4}22$	2.80	12	2.79	12	2.79	22	2.80	W
331, $\bar{5}12$	2.63	W	2.60	25	2.64	W	2.64	W
241	2.58	28	2.57	W	2.57	30	2.57	34
132							2.54	W
222-$\bar{2}03$	2.52	14					2.52	W
601, $\bar{4}41$	2.44	26	2.45	30			2.44	43
$\bar{4}03$			2.39	16			2.39	W
151	2.36	24	2.36	W			2.36	23
350	2.27	12	2.29	W			2.27	W
$\bar{6}22$	2.22	W	2.21	W			2.22	W
060	2.18	14	2.19	25			2.18	W
$\bar{3}33$, 620	2.16	30	2.15	15			2.15	28

I. Euhedral white crystals on diorite, Woodleaf Quarry.
II. Pink acicular crystals, Woodleaf Quarry.
III. Leonardite, Madsen and Murata, 1970, p. 193.
IV. Laumontite, Liou, 1971, p. 386.
(a) After Liou, 1971, p. 386.

of unreplaced microcline and sphene in a matrix of secondary prehnite, chlorite and epidote. In less altered granites only plagioclase is prehnitized, the microcline, quartz, hornblende and sphene are unaltered.

Table 3. X-ray Diffraction Powder Data for Prehnite.

	I		II	
hkl	d(obs) Å	I	d(obs) Å	I
200	9.31	12	9.24	W
110	5.27	15	5.26	19
001, 400	4.61	15	4.62	32
201	4.16	10	4.14	11
011	3.54	30	3.54	43
111	3.46	70	3.47	100
211	3.31	26	3.30	62
401	3.27	40	3.27	38
311	3.07	100	3.07	94
411	2.81	35	2.81	39
020			2.74	W
220	2.63	10	2.63	18
511	2.55	80	2.56	78
710			2.38	W
021, 420	2.36	40	2.36	22
121	2.34	23	2.34	19
611			2.32	W
002, 800	2.30	40	2.31	10
321	2.21	15	2.20	10
112, 711	2.12	10	2.12	W
402, 801	2.07	15	2.07	19
620			2.05	12
312			2.01	W
521			1.99	W
412, 811, 910	1.94	20	1.934	13
10 0 0, 512	1.85	15	1.847	12
911			1.776	17
022, 820	1.762	40	1.768	52
612, 330			1.754	W

I. Woodleaf Quarry
II. Brog, 1969, p. 600.

X-ray data for two samples of prehnite are shown in Table 3.

The other zeolites are not common, and occur only as euhedral to subhedral crystals and crystal groups on joints in the granite and driorite and in druses in quartz veins cutting the diorite. A brief description of the occurrence, optical, and x-ray data follows.

Chabazite and stilbite commonly occur together on joints in the granite (Figure 2 E). The chabazite is present as small 1-8 mm) salmon red to brownish-red and yellow to clear crystals clusters. Chabazite is also present in small druses associated with quartz veins in the

Table 4. X-ray Diffraction Data for Chabazite.

	I		II		III	
hkil	dÅ	I	dÅ	I	dÅ	I
$10\bar{1}1$	9.37	48	9.33	70	9.30	S
$11\bar{2}0$	6.92	10	6.91	20	6.94	MS
$10\bar{2}2$			6.35	10	6.32	VW
$20\bar{2}1$	5.57	24	5.55	25	5.55	M
0003	5.01	32	5.00	25	5.02	M
$20\bar{2}2$	4.69	W	4.69	W		
$21\bar{3}1$	4.34	88	4.34	70	4.29	VS
	4.27	W				
$30\bar{3}0$	3.99	W	3.98	W	3.97	VW
$21\bar{3}2$	3.88	28	3.86	30	3.86	M
$10\bar{1}4$	3.59	48	3.58	45	3.56	MS
$22\bar{4}0$	3.46	20	3.46	20	3.45	MW
			3.39	10		
$31\bar{4}1$	3.24	W			3.22	VW
$20\bar{2}4$	3.19	W			3.17	VW
$40\bar{4}1$	2.93	100	2.93	100	2.91	VS
$21\bar{3}4$	2.89	44	2.89	45	2.88	MS
$22\bar{4}3$	2.85	W			2.82	VW
$40\bar{4}2$	2.78	W			2.76	VW
$20\bar{2}5$	2.68	W	2.68	W	2.67	VW
$41\bar{5}0$	2.61	10	2.62	W	2.59	W
$21\bar{3}5$	2.50	24	2.50	25	2.49	M
$33\bar{6}3$	2.10	12	2.09	10	2.07	W
$50\bar{5}5$					1.896	VW
$60\bar{6}3$			1.87	W	1.857	VW

I. Woodleaf Quarry, colorless crystals, W=weak, less than 10.
II. Woodleaf Quarry, orange crystals.
III. Passaglia, 1970, p. 1293, number 13, powder camera, CuKα radiation. VS, very strong; S, strong; MS, moderate to strong; M, medium; MW, weak to medium; W, weak; VW very weak.

diorite and occurs as milky yellow and transparent individual crystals (1-5 mm) and crystal groups. Calcite is frequently crystallized on the chabazite. X-ray data for both colorless and orange crystals (Table 4) is very similar to data presented by Passaglia (1970). His powder camera data does reveal a number of additional weak reflections not obtained in the Woodleaf material analyzed by diffractometer.

The stilbite occurs as small light yellow to transparent tabular crystal groups radiating into circular clusters (2 cm). In wider fractures, single tabular (Figure 2 F) crystals up to 8 mm long by 2 mm

Table 5. X-ray Diffraction Powder Data for Stilbite.

	I		II	
hkl(a)	dÅ	I	dÅ	I
001, 020	9.16	50	9.1	90
$\bar{2}21, \bar{2}02, 200$	5.46	40	5.4	20
220, 222	4.67	35	4.68	70
	4.44	10		
$\bar{3}11, \bar{3}12$	4.29	16	4.30	30
041, 132	4.07	100	4.08	100
203	3.76	W	3.74	20
$\bar{1}13, \bar{4}02$	3.40	16	3.41	50
$\bar{4}03$	3.19	30	3.20	50
$\bar{4}22, \bar{1}52$	3.03	65	3.03	70
$\bar{3}14, \bar{3}51$	2.78	28	2.79	20
	2.72	W		
202			2.69	20
$222, \bar{4}41$	2.59	10	2.59	20
	2.35	W		
	2.23	W	2.26	30
	2.13	W		
	2.04	W	2.04	20

I. Acicular crystals, Woodleaf Quarry, W=weak less than 10.
II. Mason and Greenberg, 1954, p. 519.
(a) Data from Mason and Greenberg, 1954, p. 519.

wide and tabular crystal groups with the typical bow tie structure occur. X-ray data is presented in Table 5.

Heulandite is not a common zeolite at Woodleaf. It occurs as small transparent, glassy crystal cluster (2-5 mm) on joints in the granite where it is commonly associated with the chabazite and is sometimes found crystallized on chabazite. Individual crystals are less than 1 mm. X-ray data shown in Table 6 compares favorably with data obtained by Mumpton (1960).

Rare scolecite is present as circular (2 cm) aggregates of parallel acicular crystals on very thin joints in the granite. Identification is based on x-ray data shown in Table 7.

In order of decreasing abundance the other secondary fracture filling and replacement minerals are: chlorite, calcite, epidote, quartz, plagioclase, pyrite, fluorite, molybdenite, and chalcopyrite. Chlorite occurs as both dark green flaky massive aggregates and as small (0.5 cm) spherical crystal clusters in vugs of the diorite. X-ray reflections suggest a Mg rich variety. Calcite occurs as : (1) small (0.5 cm) attached light yellow translucent euhedral crystals on joints and in vugs

Table 6. X-ray Powder Diffraction Data for Heulandite

	I		II		III
hkl(a)	dÅ	I	dÅ	I	dÅ
020	8.9	100	8.9	100	8.8
200	7.9	13	7.9	20	7.8
	6.85	W	6.80	W	
001			6.63	W	6.66
220	5.98	W	5.92	W	5.93
			5.58	W	
$\bar{3}11$	5.27	W	5.24	W	5.26
310	5.10	10	5.09	W	5.08
$\bar{1}31$	4.65	25	4.69	20	4.64
	4.48	W	4.45	20	
$\bar{4}01$	4.37	W	4.36	W	4.37
	3.97	40	3.97	20	
421	3.90	25	3.89	30	3.92
			3.83	W	
$\bar{2}41$	3.72	10	3.71	W	3.73
	3.48	W	3.47	W	
$2\bar{2}2$	3.42	W	3.40	20	3.43
002					3.33
$\bar{4}22$	3.19	W			3.18
510	3.13	W	3.12	W	3.13
	3.02	W	3.03	W	
350	2.97	30	2.97	40	2.96
530, $\bar{6}21$	2.81	12	2.80	W	2.80
$\bar{5}32$	2.73	10	2.72	W	2.73
042	2.63	W	2.67	W	2.67
$\bar{1}52$	2.53	W			
	2.49	W	2.48	W	
261, 441	2.43	W	2.43	W	2.43
$\bar{2}23$			2.35	W	2.35
$\bar{6}03$	2.24	W	2.28	20	2.27

I. Small white crystals on granite, Woodleaf Quarry.
II. Mumpton, 1960, p. 356.
III. Merkle and Slaughter, 1968, photograph.
(a) Data from Merkle and Slaughter, 1968.

in quartz veins in the diorite, (2) crystals that sometimes fill prehnite veins, and (3) milky white crystals associated with chlorite. Epidote occurs as both dark green subhedral vein filling crystals up to (2-3 cm long) along fractures in diorite and as fine grained pistachio green replacement product of diorite. The replacement epidote is commonly

Table 7. X-ray Diffraction Powder Data for Scolecite.

	I		II	
hkl(a)	dÅ	I	dÅ	I
220, $\bar{2}$20	6.64	100	6.64	100
$\bar{1}$11	5.87	38	5.88	35
201			5.28	2
	4.74	80		
221	4.63	50	4.63	35
$\bar{1}$31			4.44	100
330, $\bar{3}$30	4.40	40	4.40	35
240, $\bar{2}$40	4.21	35	4.22	25
420, $\bar{4}$20	4.16	20	4.16	16
331	3.65	10	3.65	10
250, $\bar{2}$50			3.51	4
	3.35	W		
440, $\bar{4}$40	3.31	W	3.31	6
$\bar{1}$51, 350	3.23	15	3.23	16
$\bar{5}$11, 530	3.19	15	3.19	10
112, 060	3.16	12	3.16	14
$\bar{2}$02, 022	3.09	W	3.09	8
260, $\bar{2}$60	2.991	12	2.993	12
$\bar{2}$22, 441	2.938	40	2.940	30
032, $\bar{3}$51	2.891	100	2.894	80
$\bar{1}$32	2.860	70	2.861	40
$\bar{2}$42, $\bar{4}$22	2.586	15	2.588	10
$\bar{1}$71	2.480	12	2.481	10
$\bar{5}$12, 551	2.443	W	2.446	8
461	2.424	12	2.423	8
080	2.370	W	2.370	4
$\bar{3}$71	2.321	W	2.321	4
$\bar{5}$32	2.297	W	2.298	8
731, 062	2.270	W	2.273	8
$\bar{2}$62, 380	2.207	40	2.208	25
$\bar{8}$30, 801	2.171	W	2.173	6
113			2.148	2
821	2.112	W	2.113	4
$\bar{6}$61	2.085	W	2.083	6
$\bar{6}$42, $\bar{3}$13	2.035	W	2.036	6
$\bar{5}$80, $\bar{5}$80	1.993	W	1.995	4
$\bar{4}$03, 333	1.959	W	1.961	6
$\bar{3}$91, $\bar{3}$91	1.905	W	1.906	6
$\bar{1}$53, $\bar{2}$82	1.881	W	1.880	6
931	1.871	W	1.869	6

I. Scolecite, Woodleaf Quarry
II. ASTM Card 21-0831.
(a) Data from ASTM Card 21-0831

associated with blue fluorite; fluorite also fills the matrix of brecciated granite.

Other less common minerals include euhedral plagioclase crystals (5-6 mm) (An 27) projecting from small fracture in the diorite; and occasional quartz crystals (0.5 mm - 2 cm) associated with pyrite in small druses in the diorite. Molybdenite crystals (2-4 mm) occur as small plates in a small microcline dike and in druzy quartz veins with translucent chabazite.

CONCLUSIONS

The Woodleaf Quarry exposes an excellent metasomatic and hydrothermal reaction zone. The intrusive granite-quartz monzonite and host diorite are cut by prehnite veinlets and adjacent to the veinlets; the quartz monzonite and granite laumontized. Fractures in the quartz monzonite are filled with pink acicular laumontite-leonardite, and adjacent plagioclase laumontized. The solutions moving into the host diorite and diorite xenoliths laumontized the plagioclase. Replacement is complete in some small xenoliths. Single laumontite crystals and crystal groups are present in fractures in the diorite.

As the temperature was reduced, cooling joints formed in the intrusive and late stage solution crystallized the calcium zeolites in fractures. Based upon mutual overgrowths the sequence of crystallization was scolecite, chabazite, heulandite, and stilbite. The other minerals replace both the granite and diorite and are present in vugs and fractures; these are: pyrite, calcite, fluorite, chalcopyrite, muscovite (fuschite), molybdenite, albite, quartz and epidote.

REFERENCES CITED

Borg, I. Y. and D. K. Smith, 1969, Calculated x-ray powder patterns for silicate minerals: Geol. Soc. Amer. Mem. p. 122, 896.

Coombs, D. S., 1952, Cell size, optical properties, and chemical composition of laumontite and leonardite: Amer. Mineral., v. 37, p. 812-830.

King, P. B., 1955, A geologic section across the Southern Appalachian; an outline of the geology in the segment in Tennessee, North Carolina and South Carolina, in Guides to Southeastern Geology (ed. R. J. Russell): G. S. A., p. 332-373.

Liou, J. G., 1971, P-T stabilities of laumontite, wairakite, lawsonite, and related minerals in the system $CaAl_2Si_2O_8$-SiO_2-H_2O: Journal of Petrology, v. 12, p. 379-411.

Madsen, B. M. and K. J. Murata, 1970, Occurrence of laumontite in Tertiary sandstones of the central Coast Ranges, California: U. S. Geol. Survey Prof. Paper 700-D, p. D188-D195.

Mason and Greenberg, S. S., 1954, Zeolites and associated minerals from southern Brazil in Deer, W. A., Howie, R. A., and Zussmas, J., Rock Forming Minerals: v. 4 Framework Silicates: New York, John Wiley, p. 412.

Merkle, A. B., and Slaughter, M., 1968, Determination and refinement of the structure of heulandite: Am. Min., v. 53, p. 1120-1138.

Mumpton, F. A., 1960, Clinoptilolite redefined: Amer. Mineral. v. 45, p. 351.

Passaglia, E., 1970, The crystal chemistry of chabazites: Amer. Mineral., v. 55, p. 1278-1301.